UTILIZING CHEMIRESISTIVE SENSOR ARRAY FOR TRACE DETECTION OF VOLATILE ORGANIC COMPOUNDS IN SUB-PPM RANGES

A Thesis
Presented to the Faculty of the Graduate School
of Cornell University
In Partial Fulfillment of the Requirements for the Degree of
Master of Science

by
Rahul Pathak
August 2016

ABSTRACT

Trace detection of volatile organic compounds (VOCs) has been investigated extensively through e-noses and chemical sensors. Low detection limits for VOCs are desired for applications in noninvasive diagnosis of lung cancer, environmental monitoring and agriculture. Physical transducers range from nano-electromechanical systems (NEMS) resonators to surface acoustic wave (SAW) devices, transistors to chemiresistors. Most desirable characteristics like room temperature operation, short response times, high signal-to-noise ratio and high sensitivity are more pronounced in chemiresistors. Hence we adopted chemiresistive mechanism to design a sensor array for detecting VOCs in sub-ppm concentration ranges. Eight chemiresistive sensors based array was fabricated with functionalized coatings of different carbon black-polymer nanocomposites, thiol-protected gold nanoparticles and monolayer graphene transferred with poly(methyl methacrylate) on four disjointed comb-shaped platinum/titanium electrodes, patterned on silicon dioxide-silicon substrates. Sensors on dual inline package (DIP) chip carriers were mounted inside a custom machined gas sensing chamber, that was attached to a bubbler setup for real time data acquisition in sub-ppm concentration ranges. Ethanol, methanol, toluene and water vapor were detected and sensors exhibited linear chemiresistive responses with concentrations at low concentration ranges. Limit-of-detection (LOD) values for each analyte were determined by extrapolation of linear relationship of sensitivity and concentration values through the origin.

BIOGRAPHICAL SKETCH

Rahul Pathak was born on May 16th, 1990 in Bhopal, MP, India. He spent his childhood and high school years in Bhopal where his interest towards science and in particular physics was first ignited by his father, who is a high school physics teacher. Hearing bedtime stories from his father about great scientists like Archimedes and Newton made him inclined towards science at an early age. Learning how a simple physical phenomenon such as a rise in water level on stepping inside a bathtub, or an apple falling from a tree can lead to revolutionary discoveries, inspired him to learn science and mathematics more profoundly.

He entered Bachelors of Technology program in Ceramic Engineering at Indian Institute of Technology (Banaras Hindu University) in Varanasi, India in 2008. During his undergraduate years, he developed a keen interest in long-distance running and playing poker, two hobbies that he continues to enjoy to this day. In the summer of 2011, he undertook nanoelectronics undergraduate research fellowship project at University of Notre Dame, IN where he worked with Prof. Tao Wang and Prof. Lei Liu on devising a microfluidic-based sensor for detection of iso-propanol and water mixtures. This experience was pivotal for motivating him to pursue higher studies. After graduating from IIT in 2012, he worked as an Assistant Design Engineer in Mecon Limited (a Government of India Enterprise) in Ranchi, Jharkhand, India. He worked in the coke ovens division of Mecon where he was responsible for modelling, design engineering and supervising the construction of coke oven batteries for prominent steel plants in India. He moved to Ithaca, NY in 2014, where he started a Master of Science degree program in Materials Science and Engineering at Cornell University.

Dedicated to my parents

ACKNOWLEDGMENTS

With overwhelming pleasure and tremendous gratitude, I would like to thank each and every individual associated with this project. First, I would like to thank Prof Harold Craighead, my primary advisor whose insightful direction and support has been crucial throughout the entire project. I thank him for accepting me as his student and for helping me to identify interesting and relevant research topic based on my interest and abilities. I would also like to thank Prof Debdeep Jena and Prof Jeevak Parpia for their support as thesis committee members. Weekly meetings and discussions with Prof Harold and Jeevak proved to be highly useful for constant and smooth progress of the project. I would also thank Prof Frank Wise and Prof Chris Ober for helpful conversations.

I would specially like to thank Abhilash Sebastian and Roberto (Bob) De Alba of Prof Parpia group for their unconditional support. Abhilash and Bob taught me many practical skills during the course of this project. I worked with Abhilash for most of the sensor devices fabrication at CNF, CCMR and assembly in the lab. His help in photolithography, evaporation, deposition, machining and wire-bonding was tremendous. His commitment and practical approach inspired my own work ethics. Bob's help with LabVIEW and MATLAB codes for interfacing digital multimeters with a personal computer and post processing of the acquired data respectively and for performing SEM imaging was vital. I appreciate the support of Eric Nelson Smith in providing very helpful advice on making a gas sensing setup from scratch. His help in machining the gas sensing chamber and mounting the sensor devices inside the chamber was invaluable. His suggestions of generating smaller bubbles to achieve sub-ppm concentration of gases proved useful and led to good results. I also acknowledge the help of R Vinayakan, whose

help was critical for the synthesis of gold nanoparticles. His expertise and knowledge of nanoparticles synthesis and properties is commendable. I thank Gregory Smith from Cornell's environmental health and safety department for helping me verify and calibrate gas concentrations with the help of Miran Sapphire Portable Infrared Ambient Air Analyzer. I also thank CNF, CCMR and CNET staff especially Christopher Alpha, Garry Bordonaro, John Treichler, Edward Camacho, Steve Kriske, John Grazul and Brenda Fischer.

I also thank present and former members of Prof Craighead research group - Harvey Tian, Sarah Reinholt, Christopher Wallin, Jaime Benitez and Jia-Wei Yeh. I appreciate their help and friendly encouragement throughout the duration of this project. I thank Chris for showing me around the labs when I was new and I thank Harvey for ordering nitrogen gas cylinders whenever I needed more for my experiments. I also thank my friends and classmates - Suresh Vishwanath, Amit Verma, Anuj Bhargava (for the many hours spent playing table tennis), Pranav Gupta (for the miles of running and biking together), Sai Vineeth Bobbili, Phil DePond, Thomas McCune, Nathaniel Davenport, Aaron Chronister, Luke Johnston, Mary Kate Wheeler, Maggie Henderson, Bernardo Fichera, Burt Lien, Himanshu Goyal, Ved Gund, Apoorva Kiran, Reet Chaudhuri, Ashudeep Singh, Aditya Sundar, Amit Bhatia and Santosh Kalyan. Their support and company made my stay in Ithaca a bit more eventful.

I also thank my past teachers and mentors for shaping me into who I am today. Last but not the least, I thank my parents for their emotional support and for being on my side regardless of any circumstances. Let me extend my gratitude to everyone whose name I did not mention but has directly or indirectly helped me.

TABLE OF CONTENTS

CHAPTER 1
INTRODUCTION

In chapter 1, an overall motivation and discussion of state-of-the-art present technologies of chemical sensors and e-noses is presented. This is followed by chapter 2 on experimental procedures adopted by us, chapter 3 on results gathered from the setup and on discussions and analysis of the results. Chapter 4 will provide a summary of overall accomplishments and scope for future improvements.

Trace detection of volatile organic compounds (VOCs) has been a key area of research in recent years and has attracted attention of researchers in the past decade. Low detection limits of VOCs are prime requisites in research as it helps in plethora of applications ranging from non-invasive diagnosis of cancer [1, 15], environmental monitoring [3] and agriculture, by detecting insect infestation of crops [3]. Peng et al [1] identified 42 lung cancer biomarkers and demonstrated gas detection in ppb concentration ranges. Simulated lung cancer breath in their experiment consisted of mixture of ethylbenzene, undecane, 4-methyl-octane, 2,3,4-trimethylhexane, oxygen, carbon-dioxide and carbon monoxide in ppb concentration ranges. Gavgani et al [2] have emphasized the impact of VOCs in the environment and its malevolent effects. Exposure to high concentrations of VOCs has been attributed to cancer, allergies, damage to cardiovascular system and other lung diseases. They have investigated detection of methanol with concentrations ranging from 1 ppm to 1000 ppm. Emission of phytochemicals by plants as a defence mechanism and detection of these phytochemicals could lead to early detection of insect infestation. Weerakoon and Chin [3] utilized this to demonstrate a chemical switch capable of detecting ɣ-terpinene, α-pinene, p-cymene, farnesene, limonene and *cis*-hexenyl acetate.

At this point of this writing, gas sensing technology has advanced to an extent that enables detection limits as low as parts per billion concentration ranges. Devising such sophisticated state-of-the-art technologies demands high performance parameters such as high sensitivity, short response time, good selectivity, ambient temperature performance, reproducibility and excellent discrimination ability. The combination of all these performance parameters is difficult to achieve in a one transduction mechanism. Despite these, there have been systematic efforts in this area to overcome these challenges and combine advantages of one or more of the performance parameters into a single transduction mechanism. Researchers have utilized plethora of sensing methodologies for gas sensing purposes in recent years. Transducers for VOCs gas sensing can be broadly categorized in following ways:

1. Resonators based on nanoelectromechanical systems (NEMS)
2. Surface acoustic wave microsensors
3. Field-effect transistors based microsensors
4. Chemiresistors

Apart from this broad classification of transduction mechanism for organic gases, a variety of other methods are also present in literature viz. chemicapacitaitve sensors, calorimetric sensors, potentiometric sensors, amperometric sensors and gas chromatographic sensors. Discussing all of these gas sensing methodologies will go beyond the scope of the thesis. Hence, we will limit the discussion the aforementioned main first four transduction mechanisms and some examples from literature.

1.1 Resonators based on nanoelectromechanical systems (NEMS)

Baller et al [4] realized the idea of cantilever based NEMS based resonators by fabricating cantilever microarray sensors for detection of homologous series of alcohols. They were successful in discrimination of mixtures of alcohols and solvents.

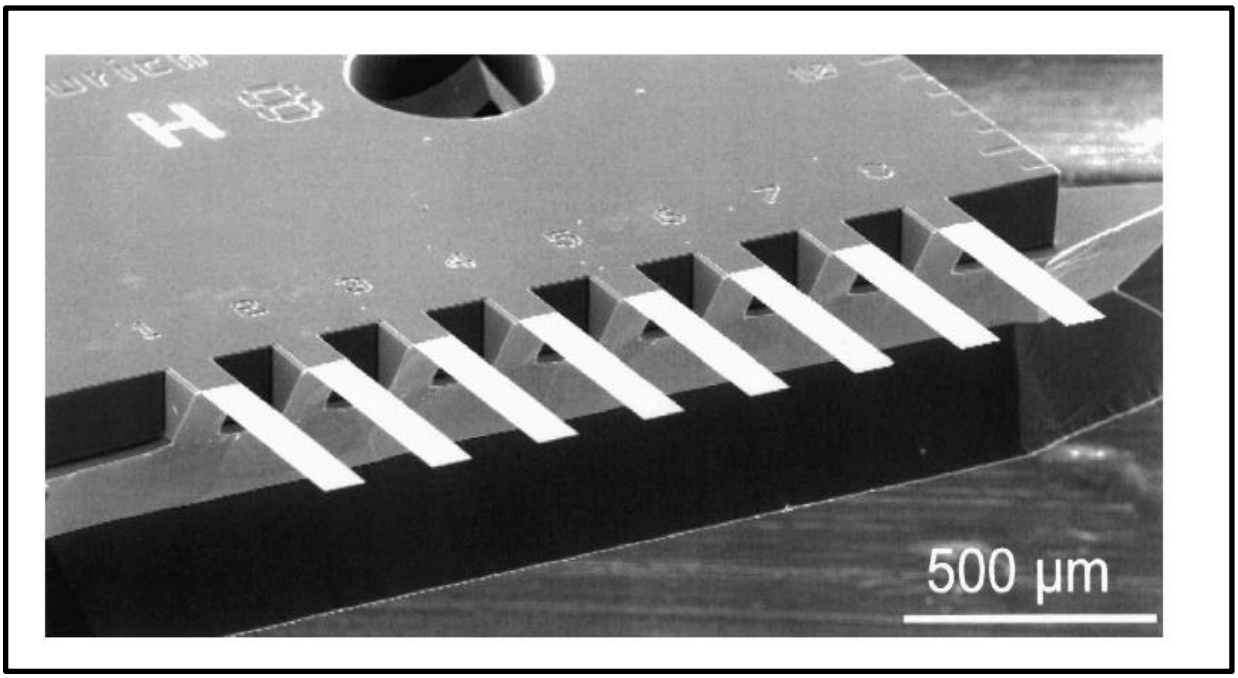

Figure 1. A scanning electron microscopy (SEM) image of the cantilever array before functionalizing with various coatings (from [4]).

Maximum deflections of individual cantilevers were measured and results were calibrated. They were able to demonstrate a quantitative and qualitative sensor array or artificial nose to create fingerprint of gases for principal component analysis and artificial neural networks recognition techniques. Their device was also claimed to be operational in various media such as ambient air, vacuum, gases and liquids. The Limit-of-detection (LOD) was reported to be 500 ppm for 1-propanol.

Kimura et al [5] also demonstrated detection of VOCs by measuring the frequency changes in the weight-detectable sensors modified with porous metal organic framework (MOF) layers. Analytes identified were toluene, acetone, octane and ethanol. Their LOD reported was 1 ppm for toluene. Similar work using HKUSK-1 MOF was demonstrated by Ellern et al [6] for detection of acetone, chloroform and toluene in concentration ranges of 1-100 ppm.

Clevenson et al [7] were able to demonstrate high sensitive microsensor based on high Q-suspended polymer photonic crystal nanocavity. The transduction was achieved by shift in cavity crystal resonance with concentration of the analyte. LOD achieved was 10 ppm for Iso-propyl alcohol. This can be seen from the illustration below.

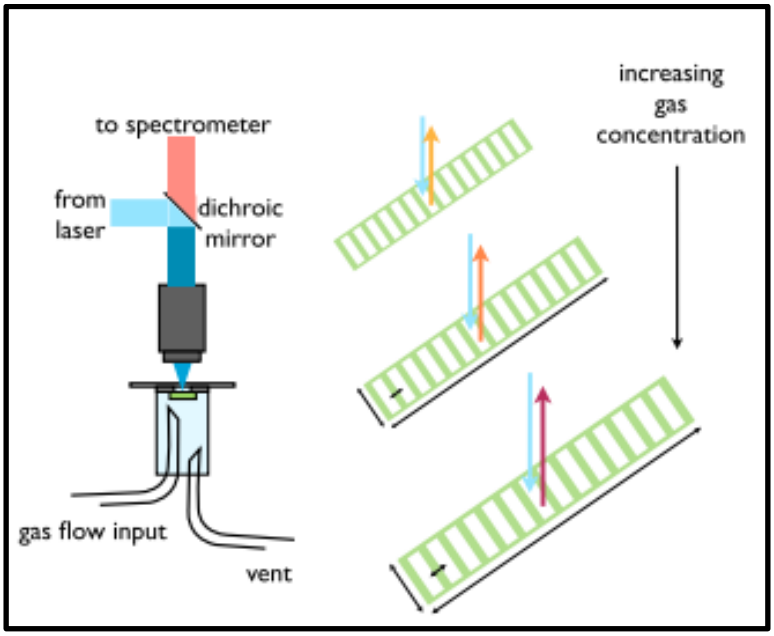

Figure 2. Experimental setup of the microsensor based on High-Q suspended polymer photonic crystal nanocavity (from [7]).

Joe et al [8] have looked into change in resonant frequency shifts of silicon-polymer composite. The sensing mechanism primarily states that for a buckled resonant microbridges, swelling of the

polymer layer alters the stress of the bridges towards more compressive as it reacts with the analyte, causing a positive axial stress and a rise in the resonance frequency. Using poly(methyl methacrylate) (PMMA) as the active sensing element, they were successful in detecting benzene, water and ethanol. The LOD for ethanol was reported to be 1.39 ppm.

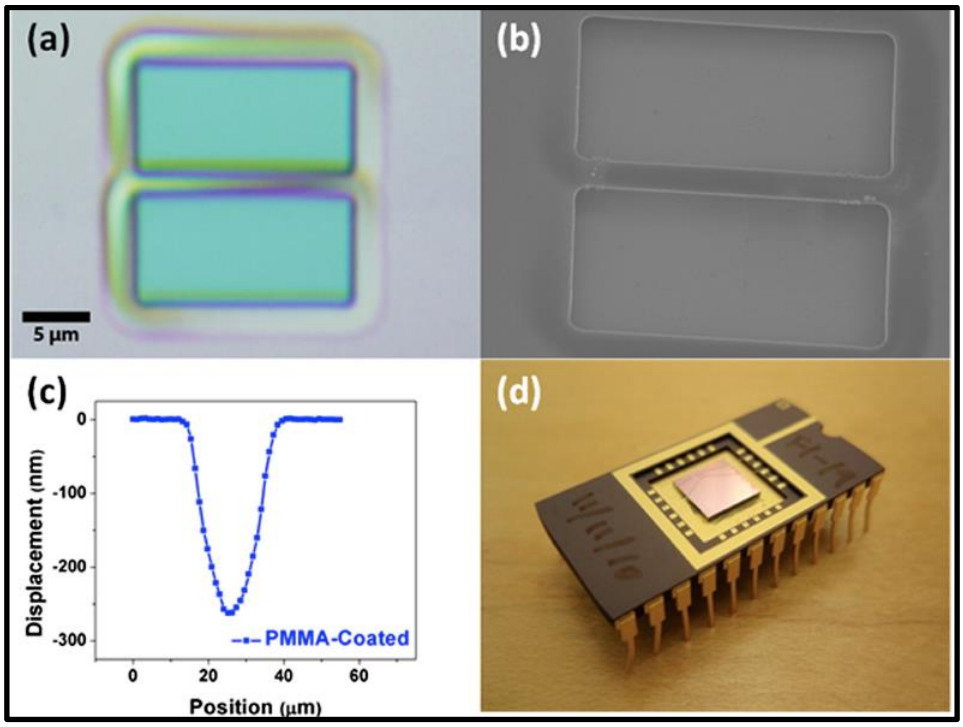

Figure 3. the optical microscopic image, SEM image, surface profile and wire-bonded chip on a dual in-line package (DIP) (from [8]).

1.2 Surface acoustic wave microsensors

Polymer coated surface acoustic wave (SAW) based devices have also attracted attention of researchers because of rapid and reversible changes and linear behavior over a large range of concentrations. Groves et al [9] devised a polymer coated 6 SAW microsensors for onsite evaluation of VOCs in water. The response of a polymer-coated SAW sensor is the shift in

frequency that is proportional to the amount of vapor exposed to each sensor. They examined a test-set consisting of dichloromethane, chloroform, 1,1,1-trichloroethane, perchloroethylene, and m-xylene in a series of experiments. Their instrument employed six 200 MHz polymer-coated SAW resonators as principal functionalized sensor units.

1.3 Field-effect transistors based microsensors

Recent advances in CMOS technologies have led to development of highly sophisticated FETs for detection of VOCs. With advances in materials science and exploration of exotic nanomaterials as we speak, there have been an ongoing interest in scientific community for further development and realization of its true potential. Christian Bur et al [10] has recently shown the use of platinum gate gas-sensitive SiC Field Effect Transistor (SiC-FET) for detection of benzene, naphthalene and formaldehyde to a detection limit of 1-2 ppb. They also show that their device responds even in a background of 2 ppm ethanol. However, they say that selectivity, i.e. detection of VOCs in a varying background of ethanol, is a major challenge since the response to 2 ppm ethanol is almost an order of magnitude higher than detection limit for VOCs.

Another work by Paska et al [11] has demonstrated the use of Si-nanowires FETs for detection of non-polar VOCs. Chen et al [12] have reported the use of graphene FETs for ethanol sensing. In their work, they fabricated a graphene FETs using standard lithographic techniques by utilizing Su-8 for the walls and top metal electrodes were present on the substrate and pressing it onto another Si/SiO2 substrate with predeposited graphene pieces. As shown in Figure 4, the SU-8 microchannels served as gas flow passage. This helped the graphene vapor to come in contact with the sensitive graphene region. They saw I*ds* change by more than 17% on exposure to ethanol environment.

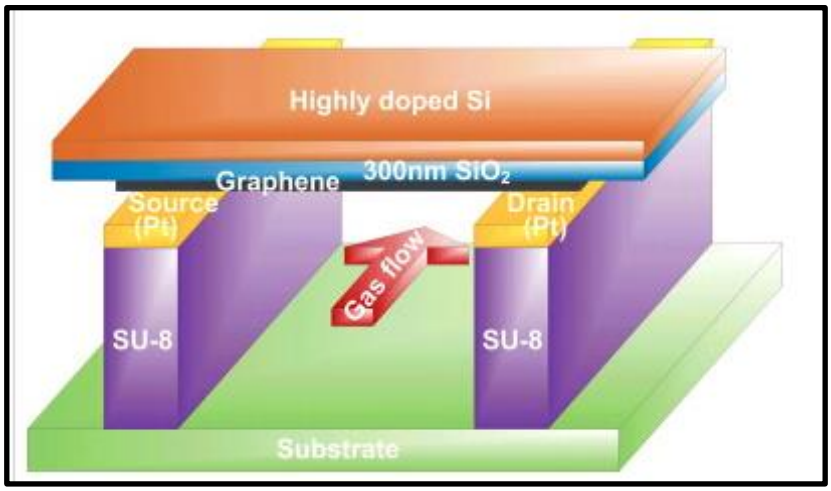

Figure 4. Schematic of the graphene FETs based sensor from [12]

In the review paper by Torsi et al [13], we see an overview of state-of-the-art sensing technologies for chemical and biological sensing using organic field-effect transistors (OFETs). In its simplest form, an OFET comprises a gate contact that is defined on the substrate which could be rigid (a silicon wafer) or flexible (plastic or even paper).

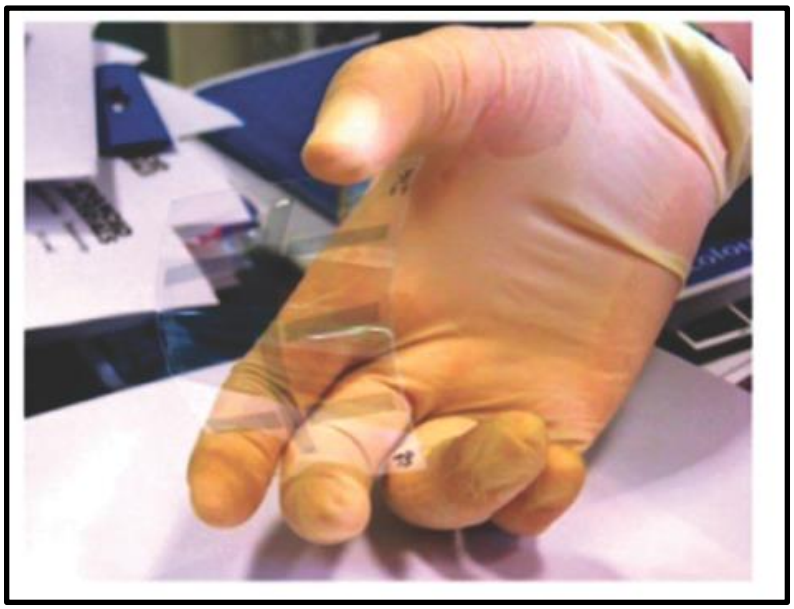

Figure 5. A picture of flexible and transparent OTFT [13]

1.4 Chemiresistors

Chemiresistors are the most common and robust categories of transducers as far as gas sensing mechanisms are considered. Functionalized layer between two electrodes act as chemiresistive sensing film/layer. Chemiresistors have been shown to demonstrate high selectivity, fast response time and reversible responses, as discussed in these examples.

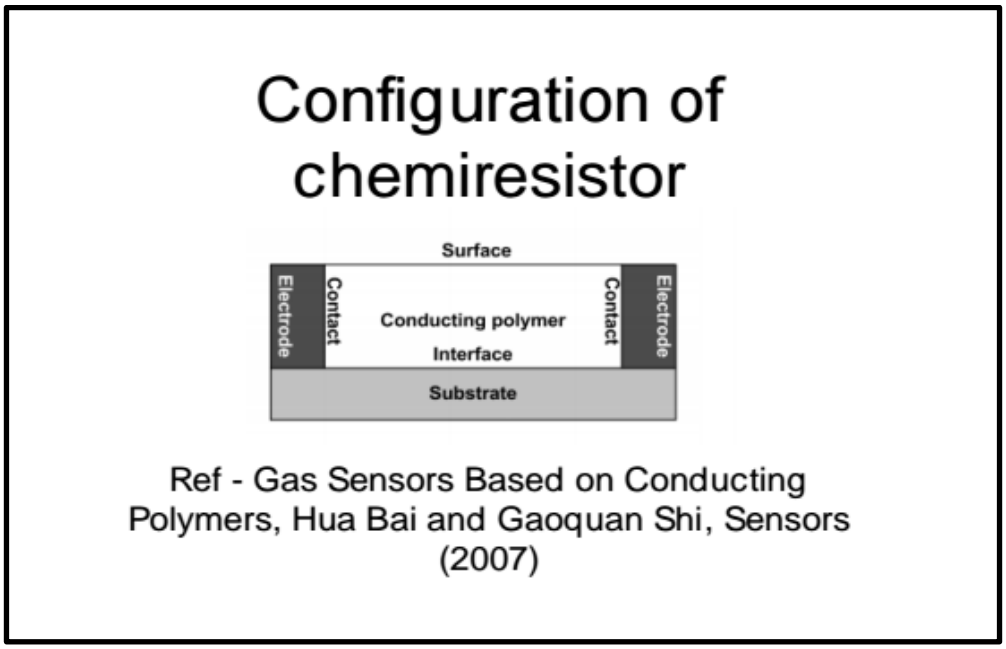

Figure 6. A typical configuration of a chemiresistor [22]

In their review, Chiu et al [14], discuss the advances of chemiresistors as active gas sensors. They broadly classify the conductive polymers based on metal-oxide semiconductor and conductive-polymer based microsensors. The table shown below, taken from this review [14], discusses advantages and limitations of each of the following categories of the microsensors.

Sensor Type	Advantages	Disadvantages
Metal-Oxide Semiconductor (MOX)	Very high sensitivity Limited sensing range Rapid response and recovery times for low mol. wt. compounds	High temperature operation High power consumption Sulfur & Weak acid poisoning Limited sensor coatings Sensitive to humidity Poor precision
Conductive Polymer (CP)	Ambient temperature operation Sensitive to many VOCs Short response time Diverse sensor coatings Inexpensive Resistance to sensor poisoning	Sensitive to humidity and temperature Sensors can be overloaded by certain analytes Sensor life is limited

Table 1. Summary of advantages and disadvantages of MOX and CP based chemiresistors, adapted from [14]

Based on these parameters, it can be clearly seen that conductive polymer systems are versatile solution for VOCs sensing applications since ambient temperature operation, good sensitivity and inexpensiveness are highly desired performance parameters and some basic prerequisites for optimal sensor characteristics. Although metal-oxide semiconductor (MOX) based sensors prove superior in terms of sensitivity and response time, poor precision and sensitivity towards humidity are the parameters that may be their limitations.

E-noses have been part of active research in the past two decades. Chemiresistive e-noses are primarily inspired by the olfactory systems of humans/mammals. The scent or smell is recognized by an array of numerous receptor cells and systematically converted to an odor signal in the brain. Each combination represents a signature “fingerprint” for a particular odor. There can be several permutations and combinations that may exist, which humans/mammals “sniff” as different odors. In a similar manner, artificial nose or e-noses also possess sensor array, transducers and a pattern recognition engine. Most popular pattern recognition engines are PCA

and ANN techniques. Mammals olfactory system may possess receptor cells in order of millions. However, practical considerations in a laboratory environment limit the number of artificial sensors for an array to a number that is far below this enormous number. There have been examples in literature that have considered e-noses systems consisting of numbers that are more realististic. Hence, these devices often possess an array consisting of 5-20 sensors. However, to increase the sensitivity and selectivity of the sensors, this number can be increased. Based on the advantages as summarized in the aforementioned table (Table 1), our motivation was to develop a chemiresistive based e-nose system for detection of VOCs.

To further study the different chemiresistive systems, they are broadly classified into three sub-systems

A. Nanoparticles-assembly based chemiresistors
B. Conductive polymers based chemiresistors (both intrinsically conducting and polymers composite systems)
C. Exotic nanomaterials or 2D-nanomaterials based chemiresistors

Nanoparticle assembly and conductive polymers systems are the broad classifications that is seen in literature frequently. Though, we have classified a third category as recently there has been a lot of interest in the 2-D materials in the research community. Although, this field is continuously evolving and still in infancy, there has been sufficient progress to categorize it separately. Let us now briefly look on to each category of chemiresistors.

1.4.1 Nanoparticle-assembly based chemiresistors

Nanoparticles based chemiresistive sensors have been explored immensely. There have been examples of works, that have demonstrated that use of, but not limited to functionalized gold

nanoparticles [1, 15] and various other metal oxides nanoparticles [16, 17] for detection of VOCs for plethora of applications.

Marion E. Franke et al [19] have discussed the conduction mechanism of conducting nanoparticles based systems. It is worthwhile to look into the underlying mechanism of charge transport in metal nanoparticles. General conduction mechanism is governed by charge transfer by hopping/tunneling between adjacent nanoparticles. When metal nanoparticles are exposed to analyte/gas as shown in Figure 7, the uptake of vapor molecules by the organic stabilizing layer, thereby affecting the charge transfer mechanism. This is a reversible process and as gas/vapor is removed from the system, the conductivity of the film comes back to its original state.

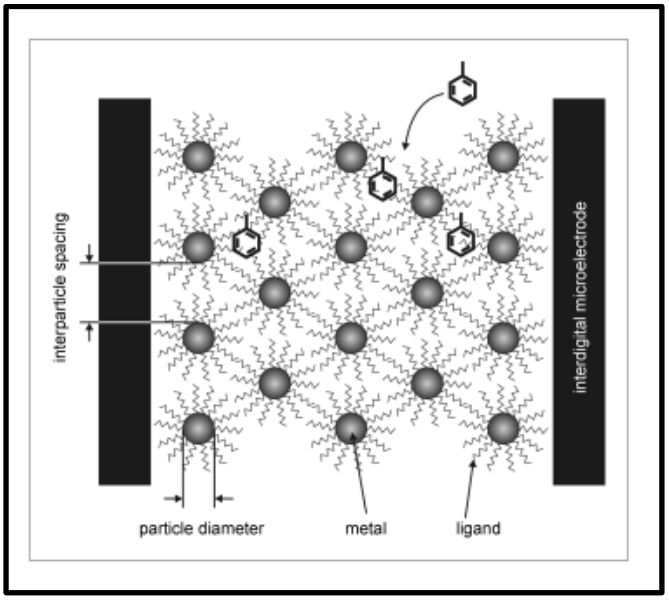

Figure 7. Simplified two-dimensional drawing of a gas-sensing film consisting of gold nanoparticles with alkanethiol ligand shells. Vapor molecules from the gas phase (toluene) absorb to the interparticle region and affect the electron-transport properties of the layer [19]

Peng et al [1] have shown the response of different functionalized gold nanoparticles based chemiresistors for application in breath analysis for diagnosing lung cancer. Not only they demonstrate sensitivity to a large array of volatile organics but they also claim very high sensitivities. Chemiresistors utilized had a variety of functionalized coatings of alkanethiols on gold nanoparticles viz. dodecanethiol, decanethiol, 1-butanethiol, 2-ethylhexanethiol, 1-butanethiol, 2-ethylhexanethiol, hexanethiol, tert-dodecanethiol, 4-methoxy-toluenethiol, 2-mercaptobenzoxazole and 11-mercapto-1-undecanol. The selectivity of each sensor was determined by the nature of these functionalized ligands attached to the gold nanoparticles. The sensor array showed fast and reversible response to variety of VOCs in a wide range of concentrations. The sensitivities reported are in ranges of 1-5 ppb for variety of compounds by most of the sensors.

Another work done by the same group [15] extends the idea of using functionalized gold nanoparticles on flexible substrates (kapton tape in this case), thereby increasing the effective detection conductivity ranges by altering the spatial orientation of gold nanoparticles. They demonstrate non-invasive detection of ovarian cancer biomarkers in the exhaled breath of the patients. This proof-of-concept work for an integrated system allows real time data acquisition and analysis of sensors based on flexible substrates. The idea of using flexible sensors being relatively new, is being explored widely at present. Although, their capability of increasing effective range of sensors is highly desirable for sensitivity, research is still not conclusive to have this approach being adopted to next generation commercial diagnostic tools. Figure 8 shown below depicts the system implemented inside a sensing chamber and strain profiles of the flexible substrates used in this work.

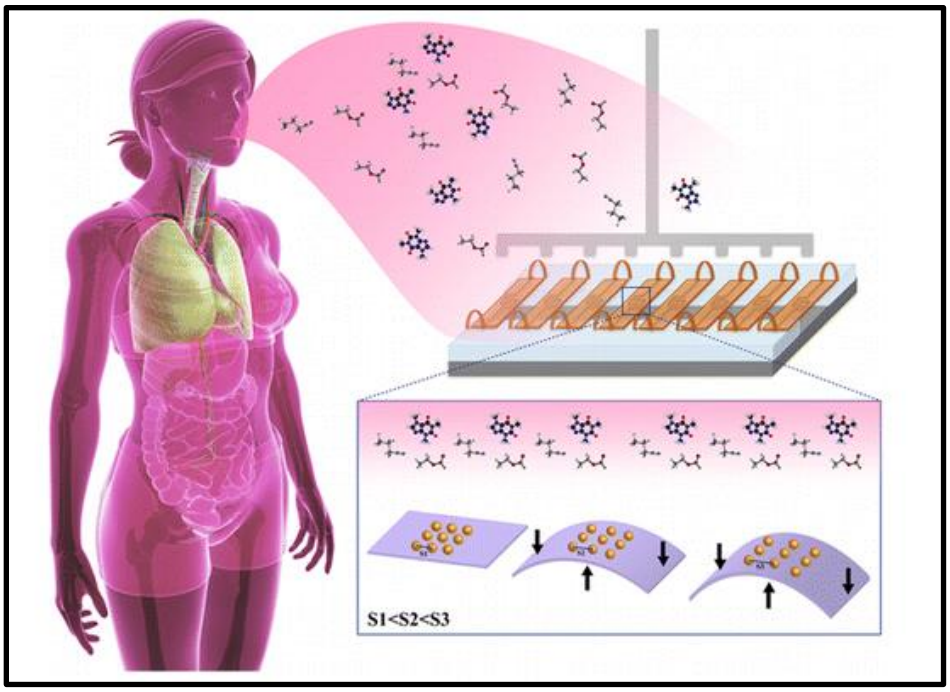

Figure 8. Sensing chamber for allowing exposure to multiple sensors to controlled VOC environment and the exerted strain on the sensors [15].

Zhipeng Li et al [16] demonstrated the use of SnO2 nanospheres as functionalized candidates for VOCs detection. The gas sensing mechanism has been described as the change in electrical conductivity resulting from the chemical interaction of molecules with the surface of metal oxide nanospheres. They demonstrate excellent response to VOCs including ethanol, acetone, chlorophenol, toluene, acetonitrile and chloroform down to concentration of 1 ppm and demonstrated LOD towards ppb ranges.

A more recent work by Inyawilert, K. et al. [17] has shown that graphene loaded In-doped SnO2 sensor is a promising candidate for ethanol detection. The ethanol sensing properties was seen to be dependent on operating temperature, In-doping and graphene loading. This study provides researchers with potential opportunity to explore on the ideas of modifying metal oxides sensing films and show interesting results on sensing properties that simple surface

modifications can induce. The modifications in the composites alter the surface area, reactive sites, surface morphology and porosity that lead to changes in response and recovery times of the sensor at the same time affecting the specificity and selectivity of the sensing devices.

Response to humidity is an important parameter to take into account as most sensors are used in ambient environment where moisture may interfere with the detection capability of these sensors. Platinum nanoparticles on a flexible polyimide substrate based sensors [18] was investigated that showed response to humidity in concentration ranges of 5000 ppm to 20000 ppm. They demonstrated that inclusion of polyimide substrate has not affected the fabrication process that was previously demonstrated using conventional substrates. The fabrication process consisted of conventional photolithography, e-gun evaporation and lift-off techniques. The second phase of deposition of "naked" Platinum nanoparticles on substrate using modified magnetron sputtering technique that enabled the nanoparticles size and density control through experimental parameters. The final step involved deposition of poly(2-hydroxyethyl methacrylate) layer, that also acted as the gas sensing layer on nanoparticles using ink-jet micro printer. This was claimed to be the first step of using polyimide substrate and further improvements in this technique can lead to cost-effective device as par with the conventional Silicon-based fabrication techniques.

1.4.2 Conductive polymers based chemiresistors (both intrinsically conducting and composite systems)

Conductive polymer systems are highly explored systems for vapor detection. They are inexpensive, robust and easily fabricated in a common laboratory environment. First implementation of conductive carbon black and polymer e-nose sensor array came from Nathan

S. Lewis et al [20], who demonstrated use carbon black-polymer resistors for applications of VOCs sensing. Vapor-sensing elements were fabricated that showed reversible change in signal with exposure to different gases. Carbon black was the conducting phase and a different organic polymer was used as the functionalized insulating phase. The total number of different polymers used for sensor array was 17. Each polymer composite sensor produced a differential response to exposure to different gaseous analytes. Nine common organic gases viz. acetone, benzene, chloroform, ethanol, ethyl acetate, hexane, methanol, 2-propanol and toluene were exposed to the sensor array in their study. The swelling induced resistance changes were measured in each resistive sensor element after exposure to gases. The resistivities of carbon black and polymer composites are explained by percolation threshold theory which states that as carbon-black content increases beyond a certain threshold, there is a sharp increase in conductivity with a small variation in carbon black concentration. Induced swelling due to exposure to analytes disrupts the conduction pathways, thereby increasing the response of each individual sensor. This suggests that sensors near the percolation threshold would give a higher magnitude of response compared to sensors having a higher carbon black concentration.

In a more recent effort to determine the limit-of-detection capability of carbon black-polymer nanocomposites for volatile biomarkers present in exhaled breath Nae Kyoung Kang et al [21] investigated responses of carbon black-polymer sensor array with various concentrations of VOCs. They identified VOCs viz. acetic acid, toluene, ethanol, acetone, n-pentane, and isoprene to have been present in exhaled breath. According to their investigation, it was determined that based on the type of polymer selected, the LOD could reach 80 ppb. 80 ppb LOD value was reported for acetic acid, 1.2 ppm for toluene, 0.62 ppm for ethanol and 20 ppm for n-pentane and 11 ppm for isoprene. The polymers used were ethyl cellulose, PMMA, PVP,

PCL, PEVA and HPC. The best sensitivity was observed with ethyl cellulose and PMMA. Lowest LOD observed with EC sensor was for toluene, n-pentane and isoprene while PMMA sensor showed best signal-to-noise ratio for acetic acid, ethanol and acetone.

The phenomenon of operating sensors near to the percolation threshold has been realized by Weerakoon and Chin [3] for detection of phytochemicals emitted by plants on insect infestation or attack of herbivores. The percolation point determined for Polyethylene-co-vinyl acetate and carbon black composite was determined at 2.5 wt% carbon black. The sensor fabricated used 4 wt% carbon-black content to obtain a chemiresistive change that is a few orders of magnitude higher when being exposed to ɣ-terpinene. This sensor was capable of detecting markers of insect infestation viz. ɣ-terpinene, α-pinene, p-cymene, farnesene, limonene and *cis*-hexenyl acetate. The LOD reported was 5 ppm for ɣ-terpinene. This LOD values was well below the volatiles emitted by plants, that are in range of 100 ppm.

Using a conductive pathway other than carbon black has been experimented and implemented in recent years. For example, Chatterjee et al [22] have implemented e-nose system constituting carbon nanotubes (CNTs) based quantum resistive sensors array. By dispersing multiwalled carbon nanotubes in different solutions of organic polymer, different sensor elements were implemented in this e-nose system. The response change was attributed to the change in motion of electrons circulating through the percolated network of CNTs. These chemiresistors were then exposed to 7 polar and 11 less or non-polar saturated VOCs to get responses from the e-nose. The set of polar VOCs constituted of water, ethanol, methanol, acetone, propanol, isopropanol and 2-butanone and set of less or non-polar VOCs constituted of chloroform, toluene, benzene, styrene, cyclohexane, o-xylene, n-propane, n-decane, 1,2,4-trimethy benzene, isoprene, 1-hexene. This system was capable of demonstrating high sensitivity

and selectivity of quantum resistive sensors for biomarkers considered for lung cancer. A small variation in CNT-CNT junctions because of the diffusion of VOCs leads to significant resistance change because of ohmic conduction substitution by quantum tunneling conduction provided that the polymers matrix has sufficient affinity for the VOCs. The discrimination ability was evaluated and found to be very good after 3D principal component analysis pattern recognition treatment.

In their review [23] of gas sensors based on conductive polymers, Bai and Shi discuss various intrinsically conducting polymers such as polyaniline (PAni), polypyrrole (PPy) and poly (3,4-ethylenedioxythiophene) (PEDOT) as active sensing layers for gas sensing systems. Examples of works have been demonstrated where Pd/PAni have demonstrated rapid and responses towards methanol. Most of the conducting polymers undergo electron transfer with analyte interaction that causes changes in resistance and work function of the sensing material/films. Other than pure redox reaction, partial charge transfer with the interacting analyte also alters the conductivity of the intrinsically conducting polymer. The electronegativity of the vapor and work function of the polymer determines the direction of partial charge transfer. Sometimes there are relatively weak interaction with many VOCs such as benzene, toluene and others as these analytes do not react at room temperature which increases the difficulty in detection through chemical reaction with conducting polymer. Though, they may undergo physical interaction with sensing polymers that may involve absorbing or swelling of the polymer matrix. Examples were demonstrated in which PPy/PMMA composite films showed response towards acetone. Decrease in conductivity was observed because PMMA encountered higher swelling as compared to PPy, thereby separating the conducting PPy. Because of their weak interaction with VOCs at room temperature, these are less reliable candidates.

1.4.3 Exotic nanomaterials or 2-D materials based chemiresistors

Interests in 2D materials especially graphene has spiked recently, due to their enhanced mechanical, thermal and electronic properties. Varghese et al have summarized recent advances in graphene based sensors in their review [24]. Though graphene can be synthesized in variety of ways, among which chemical vapor deposition (CVD) grown graphene provides large detection area and ease in fabrication of the devices. Pristine graphene is defect free and pure graphene obtained primarily from graphite exfoliation or CVD growth. Good sensitivity of pristine graphene is attributed to chemical doping by contamination from device fabrication. They discuss that pristine graphene based devices have shown sensitivity towards NO, CO2, H2S, H20 and NO2. Sensitivities exhibited towards these analytes have been very high, typically in ppm-ranges and for a select few analytes, even in range of sub-ppb.

Shishir et al [25] demonstrated this capability of graphene based by fabricating a sensor through direct transfer of graphene on paper. This example is a stepping stone for a low-cost and simple approach for the next generation devices. The lower limit of detection was calculated from comparing the noise level to the slope of responses at different concentrations of NO2. Their detection limits estimated for NO2 were 754 parts per trillion (ppt) under normal conditions and 387 ppt for NO2 in deep UV environment. They observe a slow recovery times which is attributed to strong binding of the test gas molecules to the graphene surface. Exposure to deep UV light led to reduction in recovery times to tens of seconds.

Sensing properties of CVD Graphene transferred to Silicon Dioxide-Silicon wafer was explored by Smith et al [26]. Response characteristics towards water vapor, nitrogen, oxygen and argon was investigated in a temperature, pressure and humidity controllable environment. Cross sensitivities to pressure variation and response to different gases present in the atmosphere was

also examined. The sensor response demonstrated high specificity to humidity. Then density functional theory simulations were further employed to investigate the sensitivity of graphene devices towards water.

Based on the advantages offered by chemiresistors in terms of high sensitivity, short response time, ambient temperature operation and specificity to variety of VOCs, we decided to adopt chemiresistive mechanism for our research. We have explored each category of chemiresistor - conductive polymers, nanoparticle assembly and graphene based device for sensing variety of VOCs in low concentration ranges.

CHAPTER 2
EXPERIMENTAL METHODS

Based on the advantages offered by chemiresistors for gas sensing as mentioned previously, we selected an array of chemiresistors based on carbon black-polymer nanocomposites, gold nanoparticles and graphene monolayer transferred by PMMA onto Silicon based substrates. General fabrication scheme and assembly of the sensors will be discussed in this chapter.

First section will be description of deposition and synthesis methods of sensing films and patterning of electrodes. In this section, there will be subsections that will discuss the design and patterning of electrodes, preparation of carbon black-polymer nanocomposites, synthesis of butane thiol-capped gold nanoparticles, deposition method of CVD graphene monolayer by PMMA and sensing films characterization methods utilized. Second section will be a discussion of sensor array assembly inside the sensing chamber and the data acquisition system. Assembly of sensing chamber with digital multimeter in NI environment with working of LabVIEW code for creating real time data acquisition interface on a personal computer. Third section will describe gases sampling setup and evaluation of sensing measurements. Adoption of a bubbler design to sample gas flows in desired concentration ranges using multiple mass flow controllers will also be discussed in this section.

2.1 Fabrication

The sensors were fabricated in multiple steps involving electrodes deposition, wire-bonding with DIP chips and synthesis and deposition of multiple functionalized sensing films. All works were carried out at CNF, CNET and CCMR facilities of Cornell University.

2.1.1 Patterning and design of electrodes

Sensors electrodes were fabricated on a 100 mm p-Silicon wafer having thermally oxidized 300 nm Silicon dioxide layer on the top. Comb shaped titanium/platinum electrodes were deposited on the silicon dioxide layer using standard photolithographic techniques. The electrodes were designed for taking 4-probe resistance measurement to minimize the effect of contact resistances. A general schematic image representation of the sensors design is shown in Figure 9. In their article entitled *Intimate contacts* Jena et al. [32] have emphasized on concerns related to dependence of performance of 2-D materials based devices (mainly transistors) due to high electrical contact resistances. Since the transduction mechanism being adopted by us is chemiresistive in nature, this issue becomes becomes one of the primary focus and should be carefully addressed. Also, one of the devices in use is based on 2-D material ie. graphene, overlooking the effect of contact resistance in the data can have serious effect on quality and evaluation of ultimate performance in terms of signal and sensitivity values. Specific enhancements in modifications or designs of electrodes becomes imperative in order to improve the quality of the signal and eliminate any random/electrical noise in the system. This will also eventually enhance the overall limit-of-detection capability of the system.

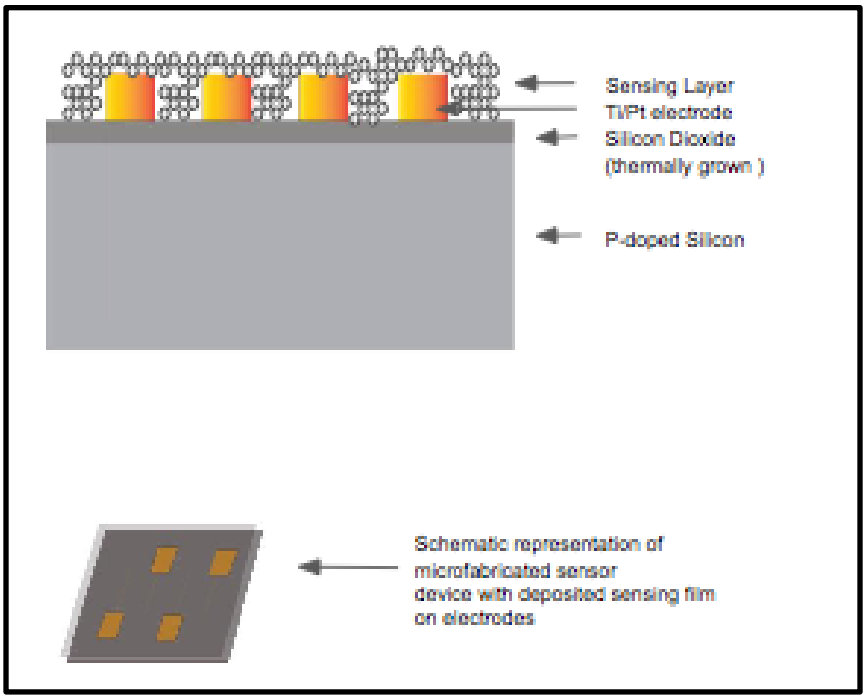

Figure 9. Illustration of the final sensor configuration with Ti/Pt electrodes, side view and top view

Previous works on chemiresistors have involved mostly the use of two-probe detection system [20, 21]. In this work, we have employed four-probe detection system, that has totally eliminated the contact resistance (however small it may be) to ensure a good signal-to-noise ratio. This design works efficiently to reduce limit-of-detection values to a lower number as it eliminates unwanted noise due to contact resistances. This design is an improvement on already established chemiresistive systems as there is no dependence on contact resistance and the signals detected come from active sensing area on the substrate. We are use graphene monolayer as an active sensing layer. Since, CVD graphene has a sheet resistance in order of kOhms [28], it is important to disregard contact resistances as this may increase the noise and overall uncertainty in the total resistance. Current leads were taken from pads # 1 and 4 while voltage leads were

taken from pads # 2 and 3. The gaps between each adjacent electrodes were of width 2 mm and was constant for all adjacent electrodes. The size of the pad was 2.5 mm x 2.5 mm and width of the electrodes was 25 microns (Figure 10).

Cleanroom recipe for lift-off process involving photolithography and deposition of metal for patterning of electrodes has been described in described in following steps:

1. Spin coated lift-off resist LOR 3A at 3000 rpm on a 100 mm wafer.
2. Soft baked at 180 deg C for 5 minutes.
3. Spin coated SPR-220-3 resist at 3000 rpm.
4. Soft bake at 115 deg C for 120 seconds.
5. Expose the wafer on MA-6 mask aligner for 7 seconds.
6. Post exposure bake at 115 deg C for 90 seconds.
7. Develop on Hamatech-Steag Wafer Processor.
8. Descum using Glen 1000 resist strip at 150 watts.
9. Loaded the wafer in e-beam evaporator and 10 nm titanium adhesion layer was deposited followed by 40 nm platinum on top.
10. Wafers were immersed in 1165 resist stripper.
11. Wafers were washed in water, IPA and acetone.
12. To remove LOR, leave the wafers overnight in 1165.

Each sensor device was diced into 9 mm x 9 mm square shapes to accommodate them into 24-pin ceramic Dual in-line package (DIP) chip carrier. Then each sensor substrate was stuck onto eight DIP chip using a double-sided tape.

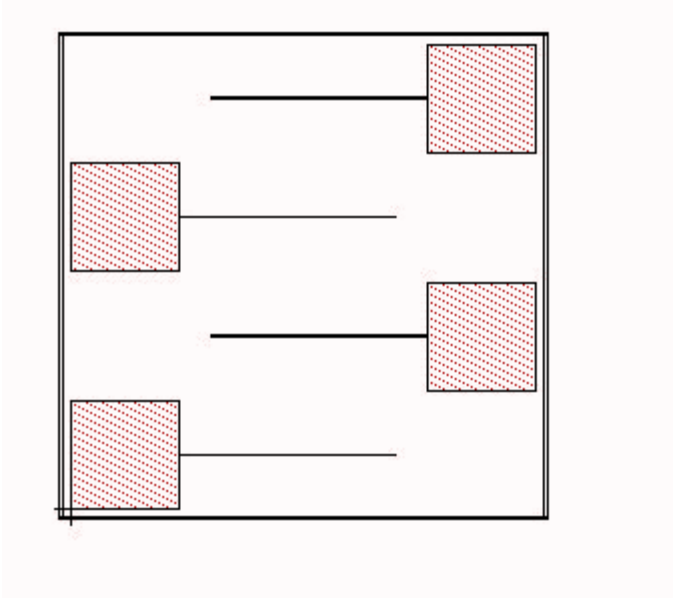

Figure 10. L-edit design of sensing electrodes with patterned electrodes

Wire bonding of the sensor substrates to DIP chip carriers was done prior to deposition of the active sensing layer except for the graphene based device, in which the wire bonding was done after the graphene transfer on the substrate. TPT wire-bonder at Cornell Center for Materials Research was utilized for this purpose. Aluminum wires were used for bonding in each case. The wires were first stuck on the DIP chips first followed by sticking the wire on the electrode pads.

2.1.2 Preparation of carbon black-polymers nanocomposites

Conductive carbon black used was Carbolac I (Cabot corporation), finely divided carbon particle of lamp black quality having a mean diameter of 10.6 nm [27]. The polymers used were Polycaprolactone (PCL, Typical Mw = 14,000, from Aldrich), Poly(vinyl acetate) (PVAC, Typical Mw = 113,000, from Aldrich), Polystyrene (PS, Typical Mw = 4,000, from Fluka), Resist grade PMMA (polymethyl methacrylate) (PMMA A4 in Anisole, Typical Mw = 495,000,

from Microchem). The solvent used was toluene (HPLC grade) for all cases. All chemicals were used as received without any modifications.

First, polymer solutions were prepared by mixing 500 mg of polymer in 15 ml solvent on a stirrer. After observing clear solution or perfect dissolution, polymer solutions were mixed with conductive carbon black particles. For making composition of 10 % (w/w) of carbon black-polymer composition 55.5 mg of carbon black was mixed in the polymer solutions while for making 5 % (w/w) of carbon black-polymer composition, 26.25 mg of carbon black was mixed into the polymer solutions. These weights were same for all polymer nanocomposites except for PMMA and PS nanocomposites. For PMMA nanocomposites, 5 ml (corresponding to equivalent weight of PMMA = 200 mg) solution was used and 22.2 mg carbon black was used. For making PS nanocomposites, 13.1 mg carbon black was added to polymer solution containing 250 mg of polymer in toluene. This was done because the bulk size of PS particles was smaller than PVAC and PCL which required less solvent for uniform mixing as compared to other polymers. The volume of solvent was 15 ml in this case. The mixture solution was homogeneously mixed for additional 5 to 10 mins. Each solution mixture was sonicated for 30 mins (using Branson 2510 Ultrasonic Cleaner) for homogeneous dispersion and breakdown of agglomerates. Final sensor fabrication was achieved by drop casting 10 μl of the solution on the already prepared sensor substrates on DIP chip carriers. Two sets of devices were fabricated with a similar concentration. First set of the device was utilized on actual sensor chip while the second set was utilized for characterization. Since the samples for characterization were taken from the same stock solution, it would demonstrate exactly similar surface characteristics as those used in devices for sensing. The as-fabricated sensors were air dried for 24 hours before utilizing them for sensing. The devices are numbered individually for identification before assembly into the sensing chamber.

2.1.3 Deposition method of graphene monolayer through PMMA

CVD graphene (bought from Graphenea) was transferred to silicon dioxide-silicon using wet transfer technique. [28] PMMA was spin-coated to a thickness of 150 nm. The copper foil was etched using copper ethant, CE-200 (ferric chloride + hydrochloric acid + water), leaving the graphene-polymer layer floating in the solution. Graphene-PMMA was washed in several baths of water (Figure 11). Next, the graphene was transferred to the substrate having already patterned electrodes. The exposed pads of the electrodes were wirebonded on TPT wire-bonder to DIP chip carriers at Cornell Center for Materials Research facility.

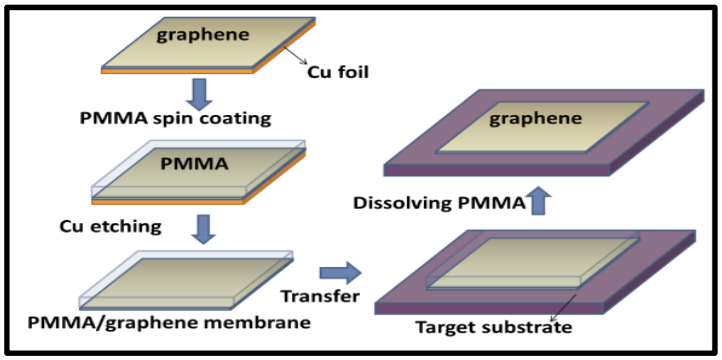

Figure 11. Summary of the process of performing wet transfer of graphene (from [29]).

2.1.4 Synthesis of butane-thiol capped gold nanoparticles

Burst process [31] All chemicals used were bought from Sigma Aldrich. HAuCl4.xH2O (MW 339.79, 107 mg, 31.5 mM, highly hygroscopic!) was dissolved in water (10 mL), in a 100 mL RB to get a light yellow coloured solution. TOAB (34.3 mM, 600 mg) was dissolved in toluene (32 mL) and added to aqueous solution while stirring vigorously for 30 minutes (organic layer turned to amber colored leaving aqueous layer colorless). Aqueous layer was removed using

separating funnel. To the organic layer, butanethiol dropwise using a syringe, while stirring. Stirring of colorless solution was continued for 15 minutes. NaBH4 (151 mg, 0.4 M, highly hygroscopic!) was dissolved in water (10 mL) and cooled in an ice bath. It was added dropwise to organic layer and continued stirring was done for 5 hours. Aqueous layer was removed and organic layer was washed with deionized water for three times (Brine or saturated NaCl solution may be used to break junk if required). Toluene was removed by evaporation. Ethanol (30 mL) was added to the solution and centrifuged (4400 rpm/30 min, cool centrifuging tube and holder assembly in ice bath prior to centrifuging) in a previously weighed centrifuging tube. Supernatant was removed and residue was dissolved in toluene (0.5 mL) and ethanol was added again (30 mL), cooled and centrifuged again as above (this step may be repeated one more time). Then centrifuge tube was dried and weighed. Butanethiol protected gold nanoparticles were dissolved in toluene. Concentration of the nanoparticles in toluene was 6 mg/ml. A small amount from this stock solution was taken for TEM imaging.

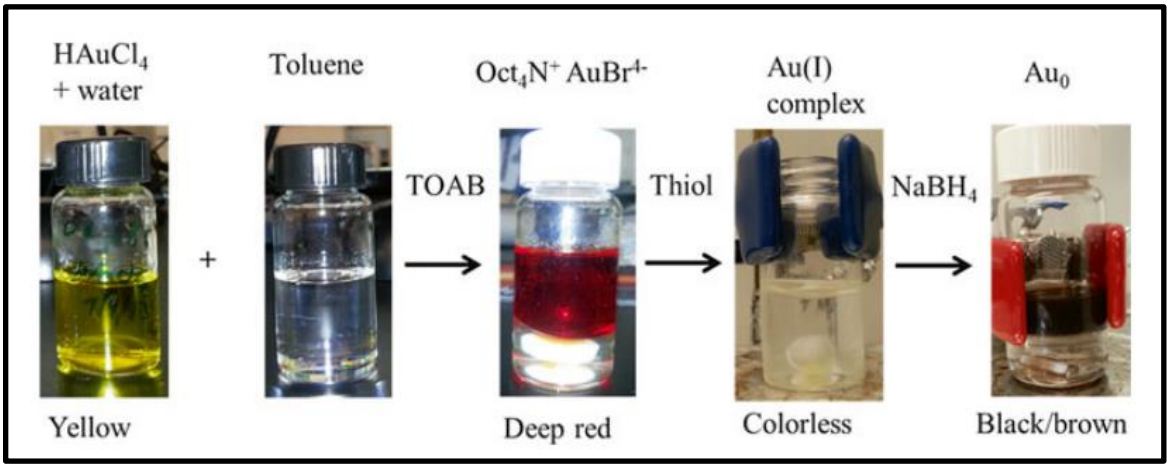

Figure 12. Figures of the reaction pathways in the phase transfer process [30]

Gold nanoparticles were drop casted on the wire bonded sensor substrate with a micropipette. Each of the drop casting step deposited 10 μl from the stock solution. The process was repeated several times until the resistance measured was between electrodes was in between 5-10 MOhms. The substrate was kept overnight to dry completely and then integrated into the gas sensing chamber.

.

2.2 Sensors film characterization

Sensing films were characterized by TEM and SEM imaging. SEM images of polymer nanocomposites are shown in the Figures 13 to 17 are shown below. TEM image of thiol-capped is shown thereafter in Figure 18.

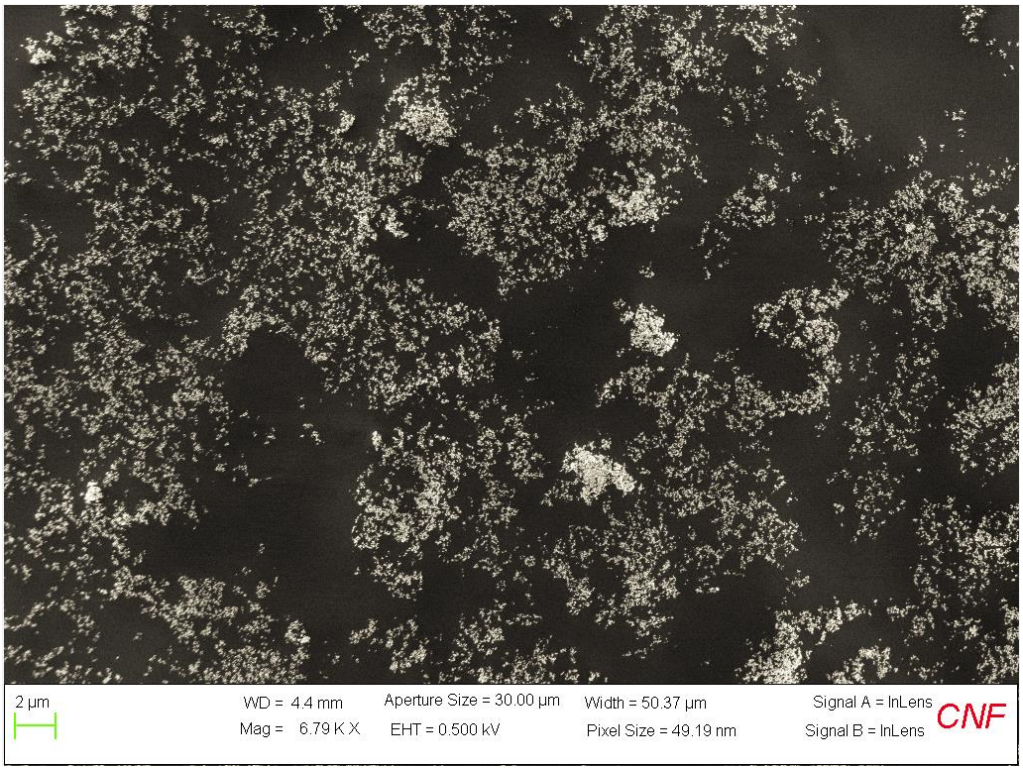

Figure 13. Carbon black (10%) and PMMA nanocomposites

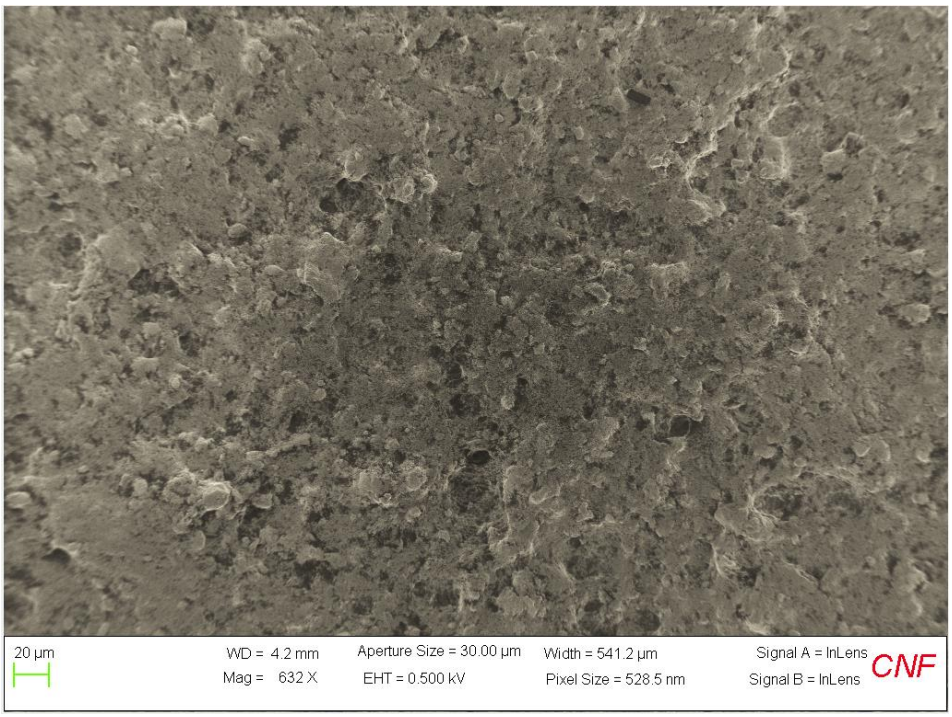

Fig 14. Carbon black (5%) and PVA nanocomposites

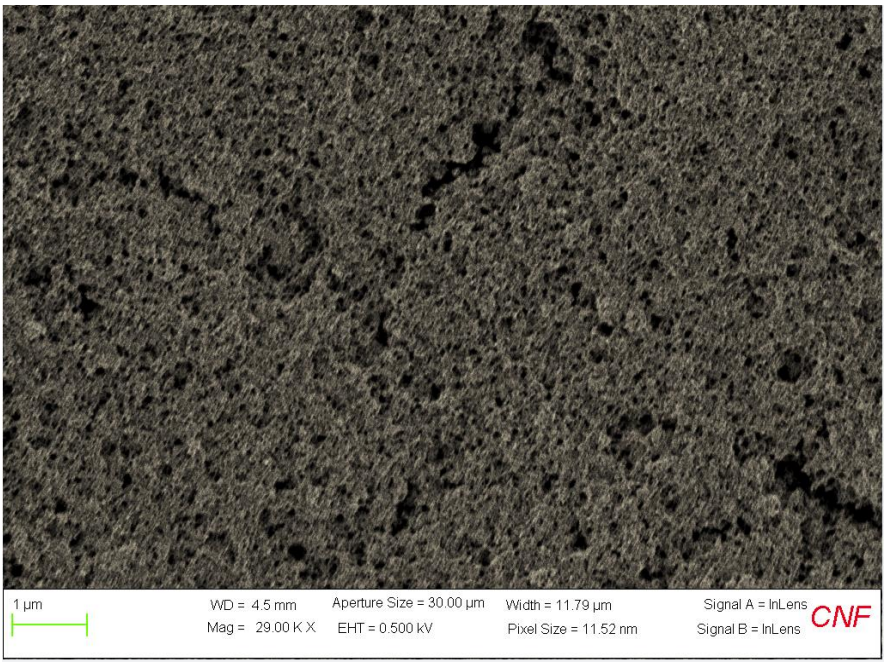

Fig 15. Carbon black (10%) and PVA nanocomposites

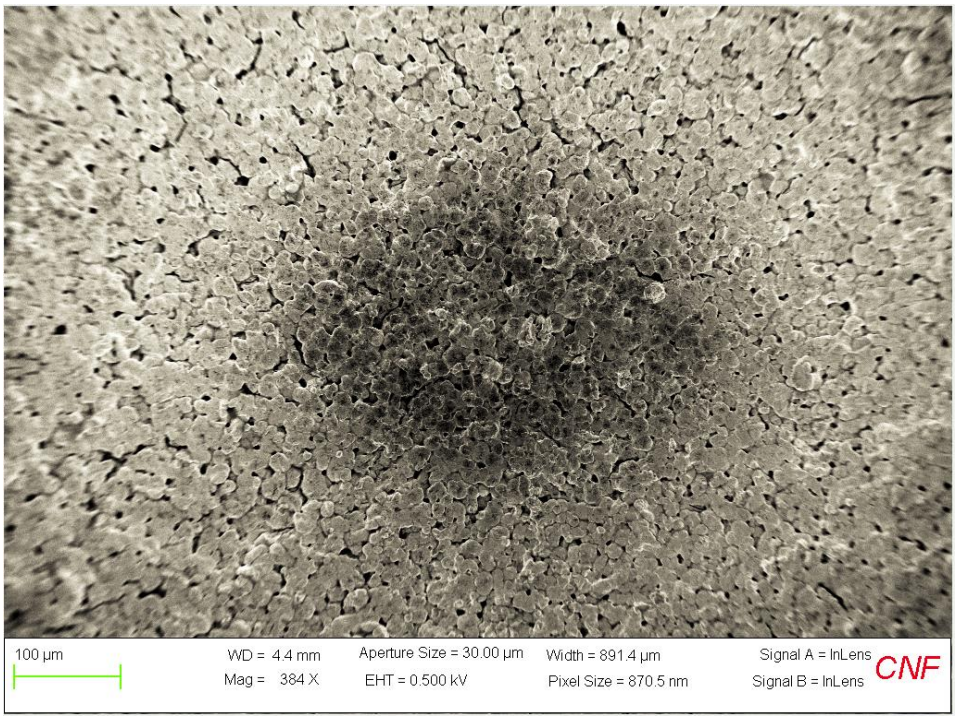

Fig 16. Carbon black (10%) and PCA nanocomposites

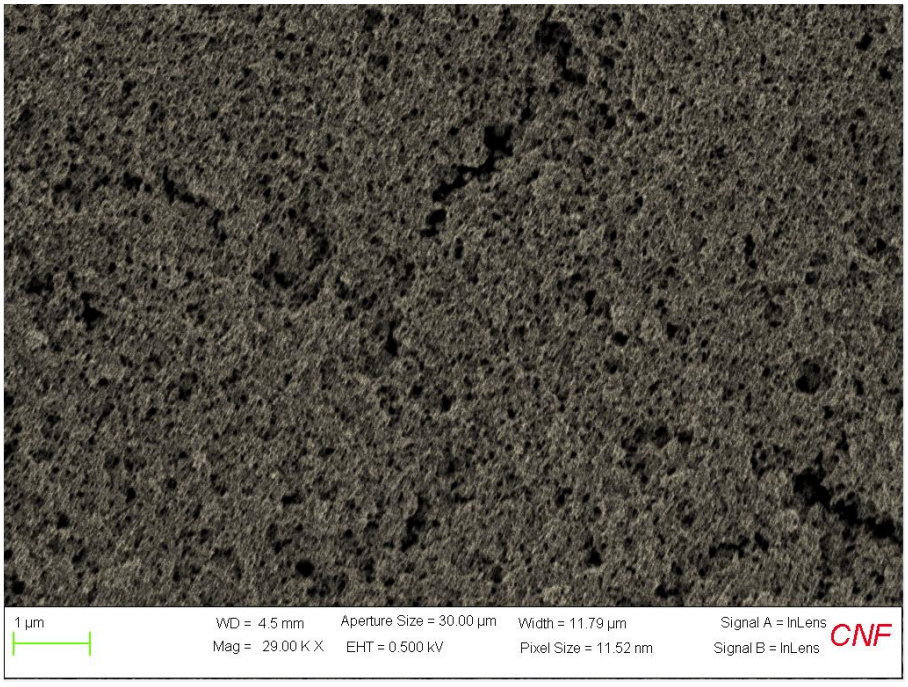

Fig 17. Carbon black (10%) and PS nanocomposites

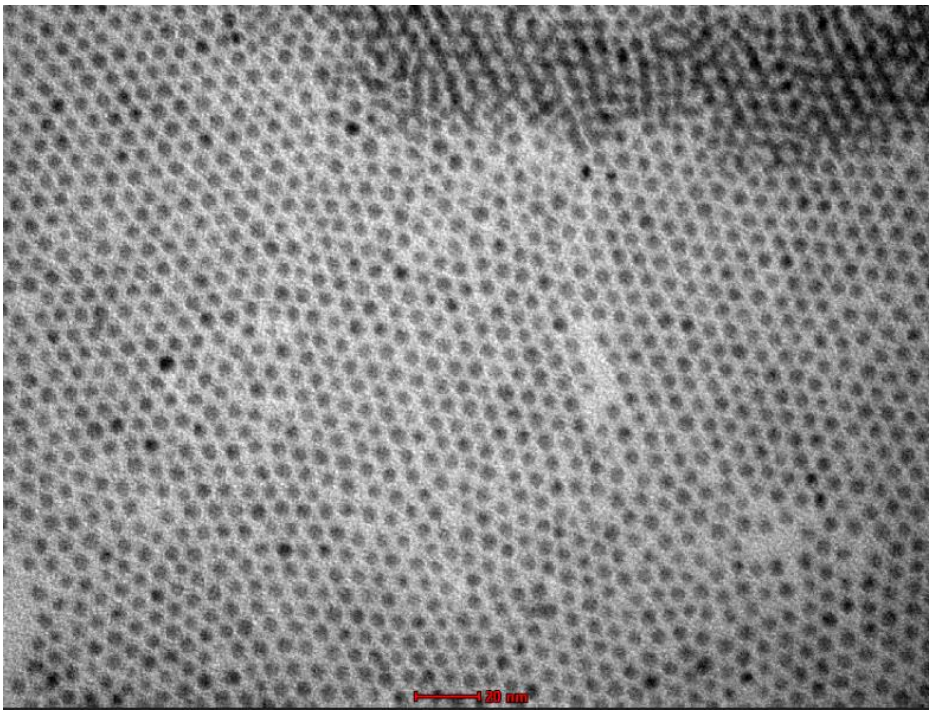

Fig 18. Thiol-protected gold nanoparticles are seen monodispersed and homogeneous.

Black areas in the SEM images are carbon black and white partch consists of the polymer matrix. SEM images show homogenized dispersion of the polymers. The polymer matrix has clearly visible voids, that are potential sites for the analyte molecules. Gold nanoparticles (Figure 18) appear not to monodisperse or form clusters.

In summary, an array of eight sensor devices was fabricated using nanofabrication and nanoparticle synthesis methods. All process did not go to fruitful completion in one trial or run and for some success was achieved after a few failed experiments or hits and trails. After observing encouraging results on test substrates, final eight devices were integrated inside the gas sensing chamber, that was custom made and specifically adopted to carry out gas sensing measurement. The final sensor array consisted of eight sensors functionalized with sensing elements as follows:

1. Device 1 - Graphene transferred on silicon-silicondioxide.
2. Device 2 - Butanethiol functionalized gold nanoparticles. (Au/BT)
3. Device 3 - Polyvinylacetate-carbon black (5%) nanocomposites (PVAC + CB 5%)
4. Device 4 - Polycaprolactone-carbon black (5%) nanocomposites (PCL + CB 5%)
5. Device 5 - Polystyrene-carbon black (10%) nanocomposites (PS + CB 10%)
6. Device 6 - Polyvinylacetate-carbon black (10%) nanocomposites (PVAC + CB 10%)
7. Device 7 - Poly(methyl methacrylate)-carbon black (10%) nanocomposites (PMMA + CB 10%)
8. Device 8 - Polycaprolactone-carbon black (10%) nanocomposites (PCL + CB 10%)

Using a hand-held multimeter typical resistance values were obtained between inner two electrodes after mounting the devices inside the sensing chamber. Device 1 had absolute resistance value in range of few hundred ohms (310.3 ohms), Device 2 in order of Mohms while all other devices showed typical resistance values in range of kOhms.

2.3 Sensor array assembly inside gas sensing chamber and data acquisition

Sensing chamber was selected specifically for VOCs gas sensing application, having a shape of a six-way cross (as shown in Figure 19) made of stainless steel. Two opposite sides were made inlet and outlet and the other four had were utilized for assembly of the sensor array. Four similar KF-50 blank flanges were machined for the sensor array setup. 24x2 holes for each one of the sensors were drilled. The holes drilled matched the dimensions of the DIP chip carrier legs. 24-pin DIP IC sockets (as shown in Figure 20) were mounted on these blanks. They were then joined using STYCAST® 1266 A/B epoxy after mounting. The flanges were kept for 48 hours for drying in ambient conditions. This was done to provide a strong and uniform sealing and

enabling the sturdiness of the system under high flow rates, that was to be applied later on. Two other KF-50 blank flanges were taken and one hole in each was drilled and swagelok fittings were attached for inlet and outlet pipes. After ensuring that it is sealed perfectly from each side and no noticeable air leaks are present, all KF-50 blank flanges were mounted with DIP chip carriers as shown in Figure 19. The pins having wire bonds were noted down and marked. Common insulated copper wire was used for electrical leads to this gas sensing chamber and connected to the appropriate pins for all sensor devices. These were connected to the two HP 3457A digital multimeters. Plug-in armature relay cards # 44491A (ordered from eBay), for each of the digital multimeter. These card were necessary as they provide simultaneous four-probe measurement capability to the system.

The multimeters were interfaced with a personal computer in National Instruments environment, with the help of GBIB-UB-HS adapter. A custom LabVIEW code (attached in Appendix I) was written to obtain real time 4 probe-resistance output from each of the eight sensors. The precision value was set at 0.001% and averaging was carried over 60 consecutive readings. The program enables simultaneous readout of resistance values for all eight devices by iterating over 8 channels for 8 sensors mounted inside the sensing chamber. The wait time between each readout was set at 3 seconds. The program was tested by performing several test runs to output best signal-to-noise ratio. The program had the capability to tune in the input current based on the absolute resistance values of each of the sensor (measured using hand-held multimeter) at the beginning of each run. Using OHMF command, maximum input and % resolution were specified by the user and the multimeter selects the one of the eight appropriate resistances ranges, accordingly input current for each individual sensor. Real time resistance values were outputted in form of a text file with column-wise raw data from all eight sensors.

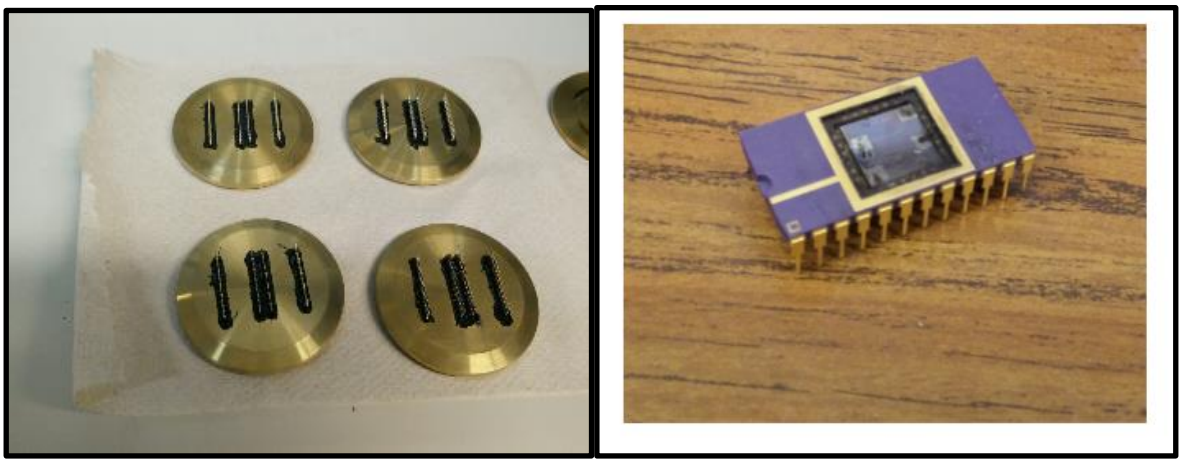

Fig 19. Hole drilled blank flanges and DIP chip carrier before mounting.

2.4 Analyte gas sampling setup and gas sensing measurements

Multiple mass flow controllers attached to a bubbler were connected to the stainless steel sensing chamber using swagelok tubing for delivery of analytes. Mass flow controllers (MFCs) were used to regulate flows in a wide concentration ranges for multiple analytes. The gas sampling setup consists of a bubbler, two nitrogen gas cylinders, mass flow controllers, carrier and dilution lines (as shown in Figure 20). The carrier flow as well as the dilution flows were controlled by adjusting the relative nitrogen flows in the main control panel. The headspace concentration of gases from the bubbler was assumed to contain saturated vapor concentration for each analyte. The design of the bubbler was such that carrier gas will enter the bottom of the bubbler and carry the analyte upwards towards the gas sensing chamber. The particular design of bubbler was adopted from Kim et al [33], keeping in mind to maximize the area of contact between the carrier gas and the analyte of interest. Maximized contact would be possible only if size of the bubbles is very small when passing through the analyte gas. This was achieved using glass frit of fine porosity at the bottom of the bubbler. Generation of smaller bubbles is essential as larger bubbles

may not be able to sufficiently carry the saturated vapor concentration being assumed for each analyte. Since there are no other rigid twists, bends or dips in the bubbler, we can safely assume that the saturated vapor concentration should be mixing at the junction of the dilution flows of nitrogen. The small bubbles can be clearly seen in Figure 21 (close-up images). Standard temperature and pressure conditions were assumed as the outlet of the sensing chamber was exposed to the atmosphere and also because no external heating or cooling was being carried out. Saturated vapor concentration values were verified using Miran Sapphire Portable Infrared Ambient Air Analyzer. The calculated values appeared to be in close conformity with the values obtained from the Analyzer. Therefore, our assumption was validated and the same concentration values were used for further calibrations of concentrations in ppm and sub-ppm ranges.

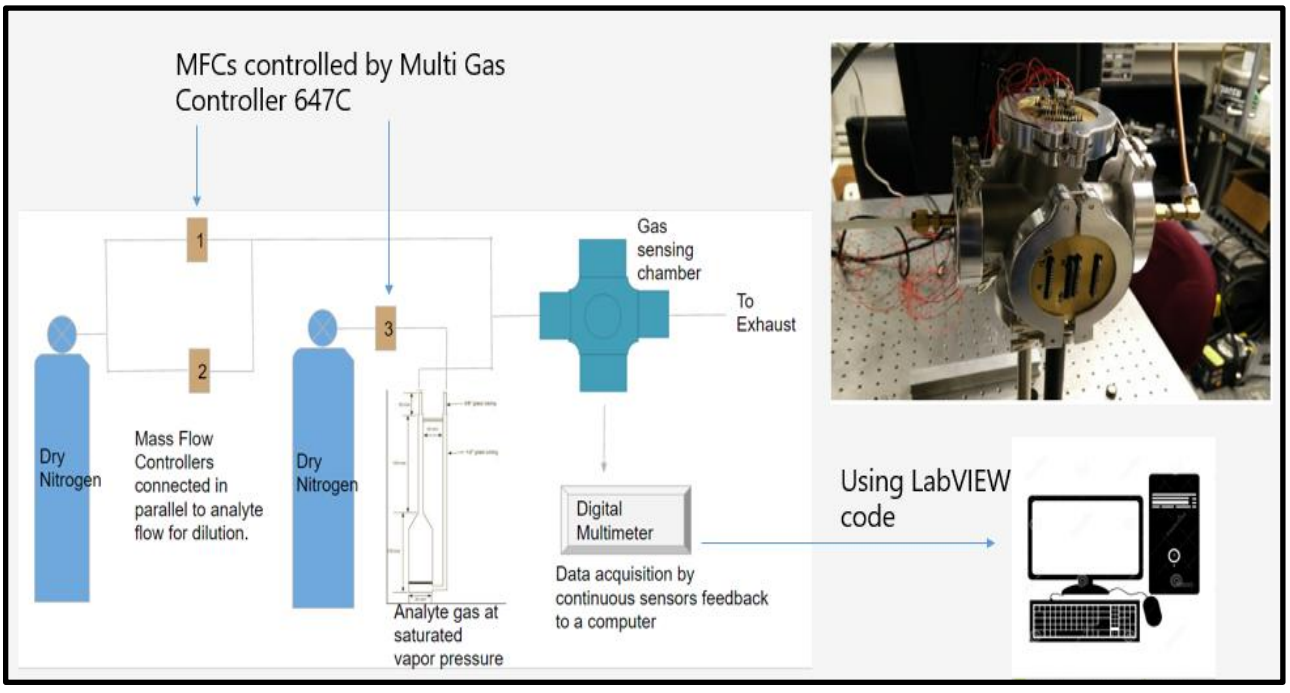

Figure 20. Final setup of the gas sensing chamber after mounting the devices and connecting the inlet and outlet tubes with computer interface to the multimeter.

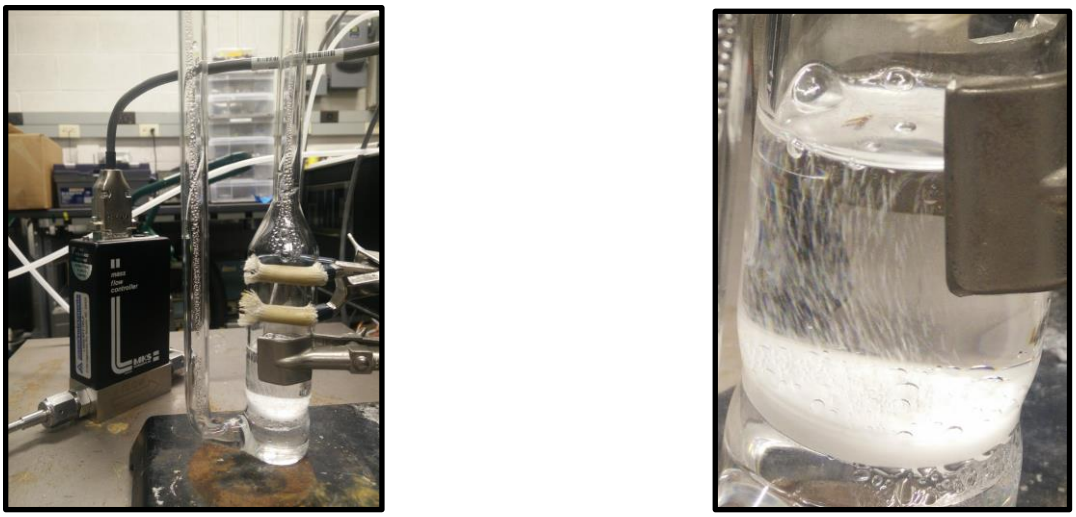

Figure 21. Bubbler configuration and formation of very small bubbles clearly visible inside the analyte liquid (water)

MFC 1 and 2 (capability of 10 SLM maximum flow rate) were responsible for dilution flow rates and MFC 3 (capability of 10 sccm maximum flow rate). MFC 3 was operated within 20-100% of the range for getting reliable measurements after multiple rounds of calibrations.

Final concentration of analyte was calculated using the equation;

$$C_{\text{ppm}} = \frac{F_c P_{th} \cdot 10^6}{P_{\text{atm}}(F_c + F_d)}$$

where

F_c = Carrier flow rate

P_{th} = Theoretical saturated vapor pressure calculated by Antoine's equation (in kPa) [34]

F_d = Dilution flow rate (in sccm)

P_{atm} = Atmospheric pressure (in kPa)

CHAPTER 3
RESULTS AND DISCUSSIONS

Using the aforementioned bubbler setup to generate concentrations in various ranges, we took measurements in fairly low concentration ranges, 0-1000 ppm for different analytes including common VOCs. The hardware setup has the capability to generate sub-ppm concentrations by adjusting the relative flows of mass flow controllers. Using a very high dilution flow may generate a positive pressure inside the sensing chamber, which is devoid of any leaks. Although most devices exhibit exponential decreasing background (as seen from Figure 22), the trend was not uniform and the devices tend to show aberrant behavior at times. For example, same device may show exponential decay along with linear rising background on a different day in same conditions. This type of behavior is commonly seen by others [35] as well and well accounted for chemiresistive devices especially for carbon black-nanocomposites. In our case, some devices tend to have a rapid response while some not so rapid that may have time constants of several minutes.

3.1 Typical behavior of devices and causes of baseline drift

Arshak et al [35] discussed the behavior of typical chemiresistors and possible causes of deviation from the ideal behavior. They describe the ideal behavior of a sensor as a first order time response. When stable baseline is achieved with the reference gas, the sensor is exposed to the analyte or odorant that causes change in output signal. When the signal reached saturation or steady-state, the odorant is switched off and a reference gas flow is maintained. After this, the sensor returns back to its baseline value. (as shown in Figure 22)

The time taken during which sensor is exposed to the odorant is called response time while the time it takes for a sensor to return to its baseline value is called recovery time. This response was attributed to the moisture intake by the devices. This is an ideal case, that is not always true for the real scenario for practical purposes. Most often, there is a drift or deviations from this ideal behavior that can arise from one or many reasons. Therefore, to compensate the drift and noise factors, the signals are manipulated in one or more of the following ways;

1. Differential drift correction
2. Relative drift correction
3. Fractional drift correction

In case of differential drift correction, the baseline is subtracted from the sensor response as a function of time. In case of relative, the sensor response is divided by the baseline. This takes into account the multiplicative drift and a dimensionless response is obtained. Fractional drift correction method employs subtraction of baseline from the sensor response as a function of time and then dividing this by the baseline. This is results in a dimensionless and normalized response of the sensor. These methods are not exhaustive in nature and it is upto the discretion of the researcher to employ the best judgement and the drift correction method based on the nature of signal and baseline drift that is being exhibited by the devices. The main mission of the researcher remains to extract the signal while compensating on the interfering factors and reduction of noise. As the drift may vary depending on the experimental setup including chamber geometry, nature and thickness of functionalized coating and ambient conditions like pressure and temperature. Non-uniform drift tendencies could also be present sometimes due to fluctuations in surface morphology of sensing films during the course of experiment.

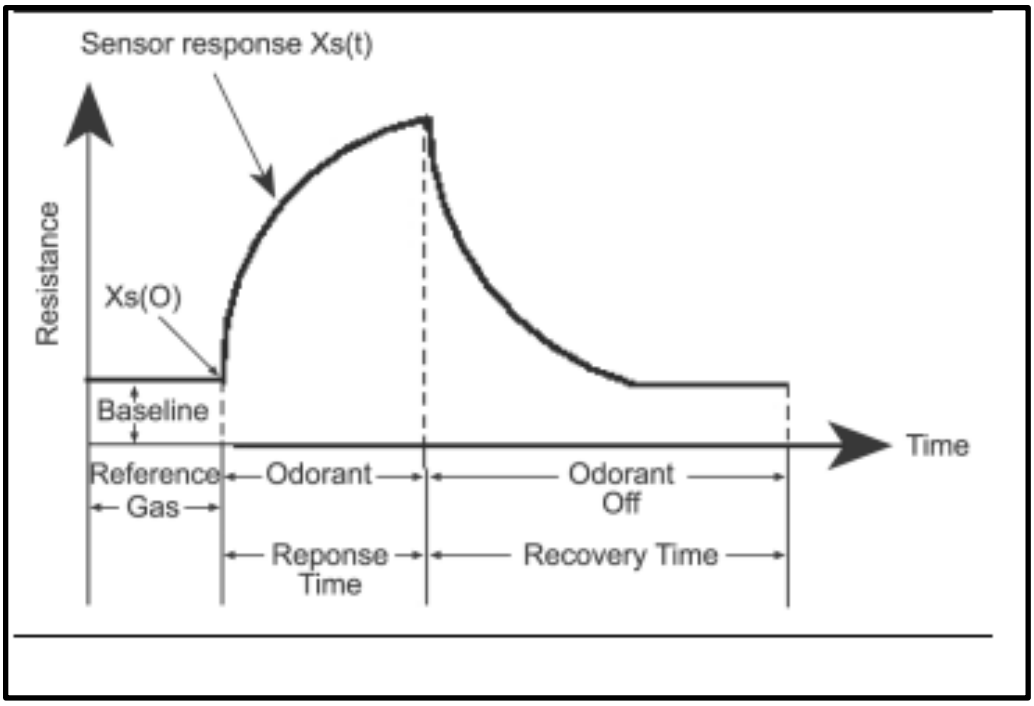

Figure 22. An e-nose sensor typical response to analyte [35]

In our case, we observed a decaying and drifting baseline with dry nitrogen gas without any analyte as seen in Figure 23. The possible causes of the baseline drift can be attributed to following factors:

- Chamber flushing and filling time
- Diffusion of analyte/background gas based on property and the sensing films
- Delayed effusion of analytes after its response-recovery cycle
- Disruption or formation of alternate conduction pathways during the course of the experiment
- Slight temperature variation inside the chamber due to use of compressed nitrogen

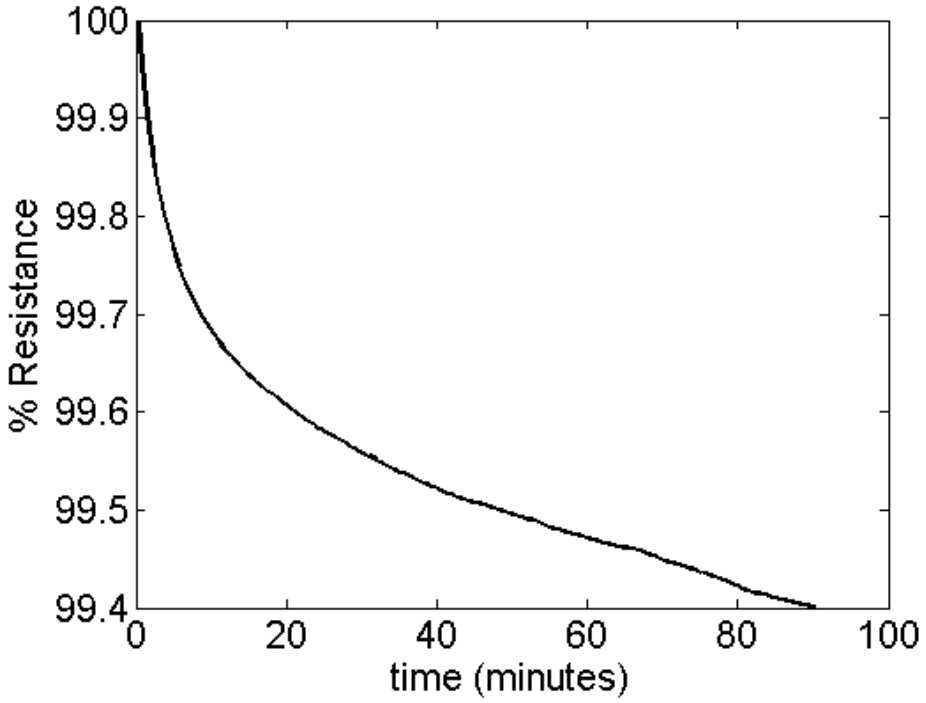

Figure 23. Drift from the baseline observed with dry nitrogen run for Device 7 (PMMA-CB 10%) as function of time.

The first effect of chamber filling time is evident in Figure 23. There is a sharp decrease in resistance with the influx of dry nitrogen. Hence this factor can be said to be the most dominating factor among all other factors. The background nitrogen run directly affects the concentrations of gases inside the chamber. Moisture content is drastically decreased and this in turn affects the value of absolute resistance dramatically. From Figure 24 and 25, we see that diffusion of gases onto two different devices, first polycaprolactone carbon-black nanocomposites and second gold nanoparticles based devices. For both types we see a similar effect in nature of signal but with polymer nanocomposites the random electrical noise is less as compared to gold nanoparticles based devices. This intrinsic property of the devices also effects the disruption and formation of alternate conduction pathways inside a device. This effect can

take place because of long term exposure of devices to very high flow rates. High flow rates may degrade the surface morphology of the device and also cause a slight pressure variation inside the chamber, making it a slightly above the atmospheric pressure. This would in turn affect inter-particle spacing and formation of agglomerations leading to change in conduction pathways. Over a long run, temperature variation of the sensing film due to continuous flow of dry nitrogen could cause a systematic variation in the resistance values.

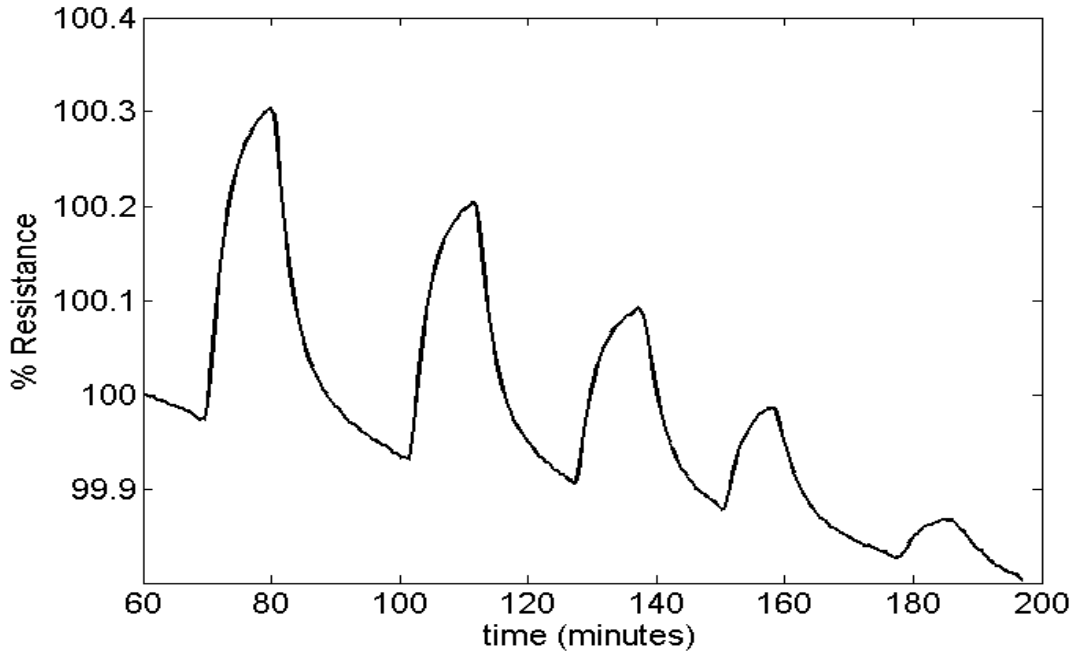

Figure 24. Real time response of Device 4 (PCL + CB 5%) as a function of time at different concentrations of ethanol ranging in between 1000 ppm and 200 ppm.

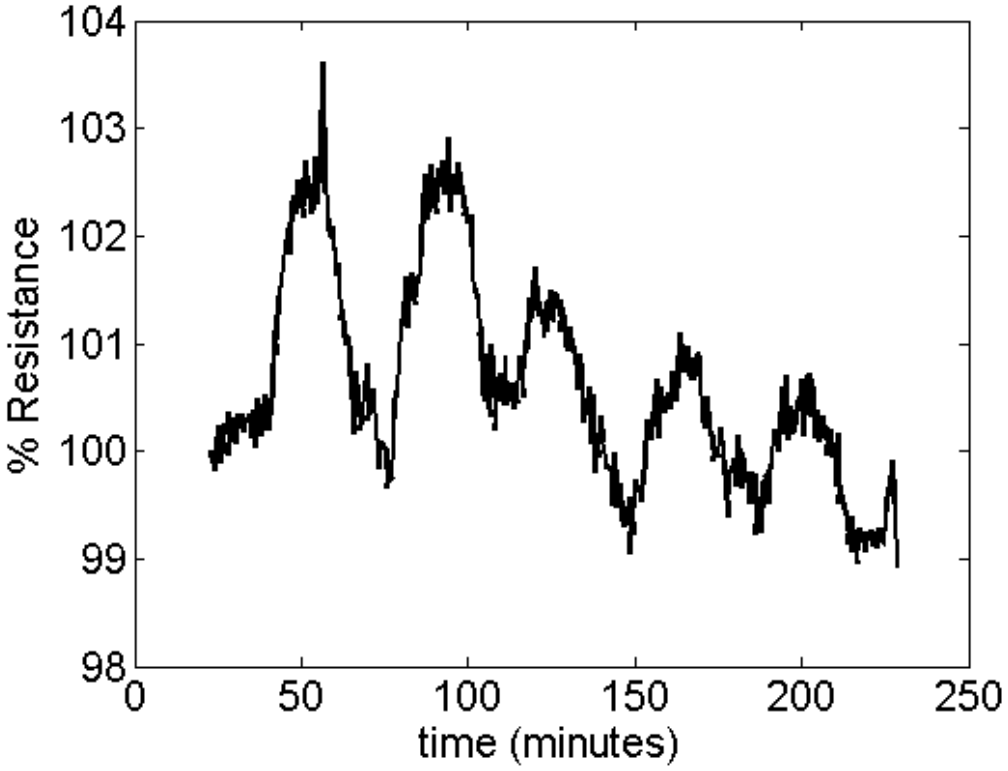

Figure 25. Real time response of Device 2 (Au/BT) as a function of time at different concentrations of ethanol ranging in between 1000 ppm and 200 ppm.

3.2 Fitting of raw data and background subtraction method

Due to the aforementioned reasons discussed, data points during for the start of the experiments were neglected and after observing a somewhat stable background, analyte was introduced inside the chamber. This disregarded the drift being caused by the most dominating factor i.e. chamber flushing and filling with the dry nitrogen. Though, other factor were still in effect, we achieved a stable enough response on which background subtraction could be implemented.

The rise and fall of the response was assumed to be exponential with a linear term (drift-dependent) on the basis of nature of the signal exhibited. While most devices show very smooth

behavior and noise free raw data, one device (Au/BT) tended to show very noisy behavior (Figure 25). Since the overall nature of response was seen similar in all categories of devices, we decided to use a single model for data fitting in polymer composites, gold nanoparticles and graphene based devices. To overcome the baseline drift and compensate for the noise exhibited by the devices, we adopted a exponential fitting function with a different rise and fall time constants depending on the gases absorption and desorption rates but it mostly governed by the chamber filling time (similar to what we observed with the background flow). The output signal was converted to a percent form by taking the initial value to be at 100%. This was done in order for enabling the fitting program to handle extremities of absolute resistances values, that may vary in the diverse range of a few ohms to MOhms. This methodology also enabled data visualization and comparison more efficient. Since the raw data behavior was observed to have an exponential decay and rise along with a linear background, each segment cycle was assumed to start at the point of switching on, switching off and ended just before the starting of switching on the subsequent gas concentration. All saturation fractional resistance in the output values at zero ppm concentrations was assumed to zero. Based on these assumptions, each segment fitted to this response function using a MATLAB code (attached in Appendix II);

$$y(t) = (y_0 - y_{sat})\, e^{-(t-t_0)/\tau} + y_{sat} + Y_{BG}(t)$$

Where y_0 = initial resistance value (percent)

y_{sat} = saturation resistance value (percent)

t0 = segment start time

$\tau 1$ and $\tau 2$ = rise and decay time constants

$Y_{BG}(t)$ = linear background as a function of time (percent)

Assuming y_{sat} values of 0 ppm are equal.

The fit was plotted with differential percent change of the resistance at t = 0, though following equation y = (delta R/Rb) x 100. The saturation values were assumed to be equal at zero analyte flow rate and y_{sat} was forced to be zero at zero concentration of the analyte for each concentration range. The $Y_{BG}(t)$ was then subtracted from the fitting function in order to accurately extract the signal from each of the sensor. The fit method is unique and could be said to be a crude combination of differential and fraction background correction methods as discussed at in section 3.1. The implementation of this method on the raw data resulted in good fits. Figure 26. shows us the fit obtained by implementing the fit equation on the raw data shown before (in Figure 24). Good superimposition of solid red and black lines gives us the impression of good possible fitting. There are only a minor patches of the raw data where the fitted line does not superimpose the raw data denoted by solid black line. Next the linear background is subtracted from this solid red line to obtain the dotted red line. This dotted red line will be utilized for further manipulation for extracting sensitivity values. We also see that segmented linear background has more or less same slope throughout different concentrations. This observation is specific property of device. In some other devices, the slope of this linear background also drifted in the course of the experiment. Hence, our model served quite well in effectively separating the linear drift segment throughout the experiment. The linear drift compensation is very effective and hence we obtain well defined signal peaks that are solely due to introduction of the analyte. This model also works efficiently for the device showing relatively higher noise levels than others. Also, the fitting method and determination of sensitivity needs to have a uniformity with all devices to withdraw conclusions and comparative analysis, the same program was utilized for data analysis for all devices for homogeneity and uniformity.

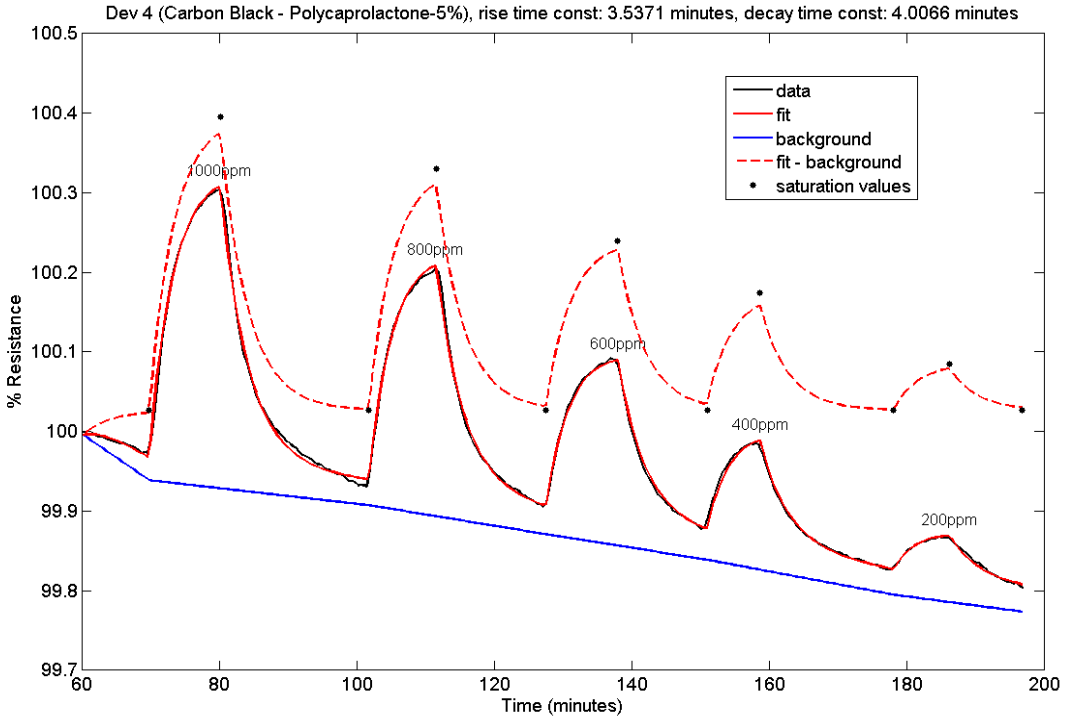

Figure 26. Fitted data is in red in the raw data from Figure 22 overlapping the raw data and dashed red is the graph obtained after background subtraction.

From this extracted red-dotted line, sensitivities values were determined. The y_{sat} values at zero ppm values were denoted R(baseline) and the y_{sat} values at the peaks were assumed to be R(max) values at the said gas concentration. The basic definition of sensitivity states that observed change in output with a known change in input. So, sensitivity was defined as,

$$S = \Delta R(max)/R(baseline)$$

where $\Delta R(max)$ is the difference of R(max) with the R(baseline) at the known gas concentration.

The sensitivities values obtained from the Figure 26. run of ethanol at various concentration ranges of 200 to 1000 ppm was plotted and the behavior of the same Device 4 (PCL + CB 5%) is shown in Figure 27. below. The linear dependence of concentration of

sensitivity with concentration is obtained. The data obtained from other sensors were consistent with this observation and provided us a foundation in understanding behavior of chemiresistive sensors in low concentration ranges.

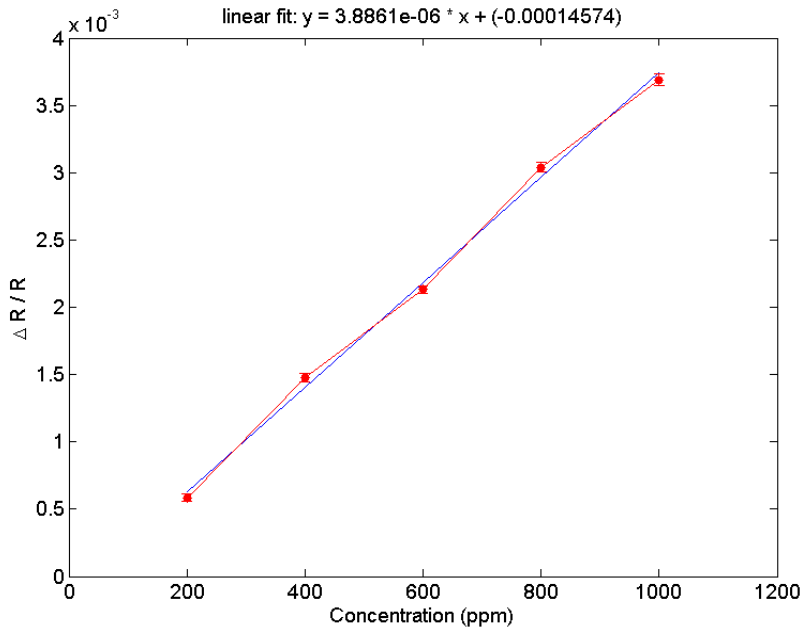

Figure 27. Linear behavior of sensitivities shown over a range of concentrations.

Another MATLAB code (see Appendix III) was written for signal processing by performing tasks like importing the text file (containing raw data), using the fitting function to subtract the background, calculating the sensitivity values, storing and plotting all values of the array for all devices. User would have to specify the initial times that should be omitted, approximate times where the gas concentrations were changes, approximate time constants for response and recovery and wiggle room for gas concentration change times. Based on these parameters, best fit was performed and sensitivity values were calculated for each experimental run.

3.3 Ethanol run and characteristic behavior of sensors over a wide concentration range

After effectively understanding the behavior of the sensors and defining a model for background compensation and sensitivity analysis, it was imperative to experiment and evaluate performance of sensor array with different analytes. Systematic studies with ethanol was undertaken for different concentrations and is being discussed in this section. First, ethanol measurement consisted of concentrations of 1000 ppm to 200 ppm in uniform decreasing intervals of 200 ppm. To corroborate the behavior of devices that would produce similar results in increasing order of concentrations, measurements were undertaken in reverse order but in a non-uniform interval. This second set of measurement with ethanol was done in a 9-hour time interval, starting with sub-ppm concentration ranges, intermediate concentration ranges and relatively high concentration ranges. Raw data for Device 3 (PVAC - CB 5%) is shown in Figure 28. The linear background drift can be seen to be directly related to the background flow of nitrogen. In sub-ppm concentration ranges, the background flow of nitrogen was kept at 15000 sccm. This flow rate is relatively high. When the background nitrogen flow is decreased to 3000 sccm for subsequent sets of measurements in intermediate and higher concentration ranges, we see the background drifting upwards. Thus, this indicates that flow rates of background nitrogen are impacting pressure and temperature inside the chamber thereby affecting the background behavior of the devices. To see if this is due to background flow, the background was increased to the initial value of 15000 sccm for a short period of time after 1st set of measurements in sub-ppm ranges. The kink in Figure 28 after the first set suggested that this behavior would be reproducible if the flow rate were continued to be increased for some more time.

Increasing concentration of ethanol from 10.5 ppm to 900 ppm (raw data)

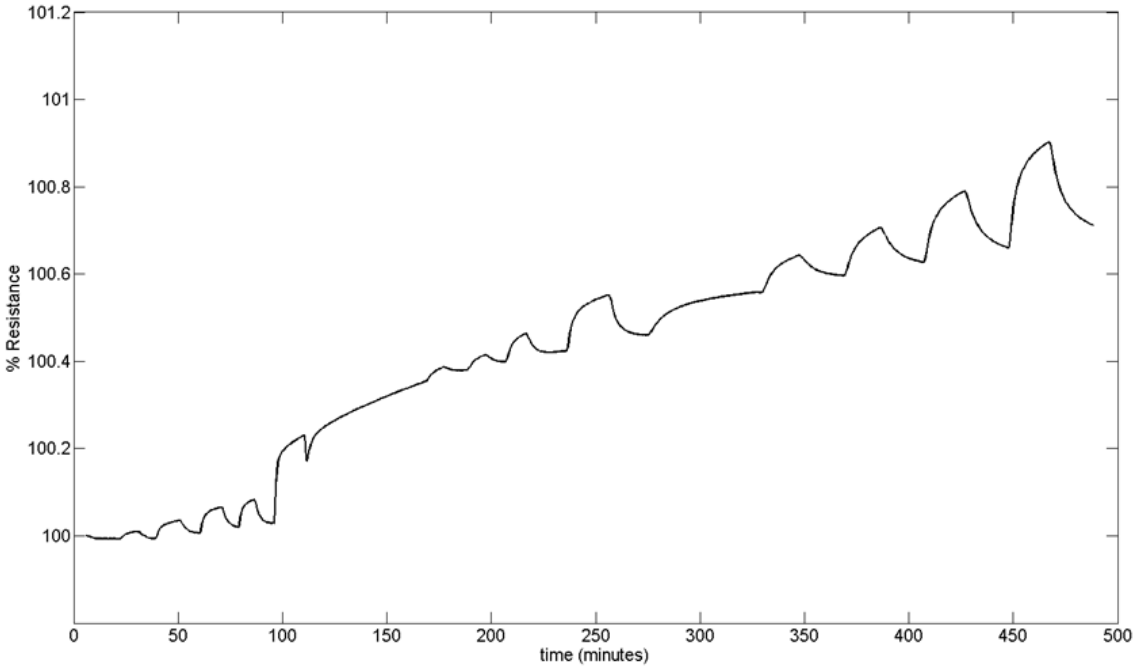

Figure 28. Raw data for 9-hour run of ethanol done from 10.5 ppm to 900 ppm non-uniform increment for Device 3 (PVAC + CB 5%), showing a clear positive linear drift.

The similar trend was observed when the transition from 2nd set of measurements in background flow of 3000 sccm to the 3rd set was made to a background flow rate of 600 sccm. The nature of change was quite pronounced in all the devices regardless of the composition of sensing films. Though for some devices, the direction of the change did not correspond to what was seen for this particular device. For graphene device, the background initially had a sharp decreasing trend and on further decreasing the background flow did not bring about a pronounced change as we see in this device. The gold nanoparticles based device also showed a similar trend. Each of the other different polymer composite devices also behaved independently.

The behavior of device 3 (shown in Figure 28) and device 6 remained to be similar in nature. Both the devices had similar polymer content (PVAC) but different carbon-black percent compositions. Thus, this is a clear indication that the specific behavior of the device is directly related to the active functionalized coating present. There could be some moisture diffusion or effusion phenomenon still be going on leading to continuous change in conducting pathways and thereby affecting the overall background behavior of the devices.

Sensitivity vs concentration values were plotted for each device in different concentration ranges. Based on the data obtained from 200 to 1000 ppm runs, straight lines were fitted to the various segments of the run. These datasets were also found to be fitted well with the straight line. The slopes of the three datasets were also found to be in similar order of magnitudes. Although, the sensitivity values at the lowest point of one set tended to be lesser in magnitude as compared to the sensitivity values of highest point of the adjacent dataset. As seen from Figure 29, the least sensitivity value on the blue line is seen to be below the maximum value from the green line. This could have two explanations; first, there can be inaccuracies in the delivered concentrations values due to calibration of mass flow controllers or second, there is a pressure increase that affects the thickness of sensing films, thereby proving it hard to “stitch” the consecutive datasets together. The first factor was minimized by calibrating the mass flow controllers before taking each measurements and ensuring its reproducibility. This was accomplished by using a graduated cylinder for smaller flows (a few sccms) and commercial gas flow meter for larger flows (a few SLMs). It was found that smaller flow tended to be accurate and reproducible for flows greater than 50% of full scale range of 10 sccm. For flows below 5 sccm, there was always an uncertainty in calibration. The standard deviation from the mean measurement was found to be around 5%. Thus, to mitigate the discrepancies and unaccounted

error between different sets of measurement, further measurements were decided to be taken in a similar background flow. This would ensure that the films are under the same physical conditions for each measurement and the sensitivities values obtained would be solely due to variation in analytes flows. Using higher flows of background nitrogen would also decrease the overall uncertainty in the absolute net concentration, if any calibration error would have been going on in the mass flow controller producing smaller flows.

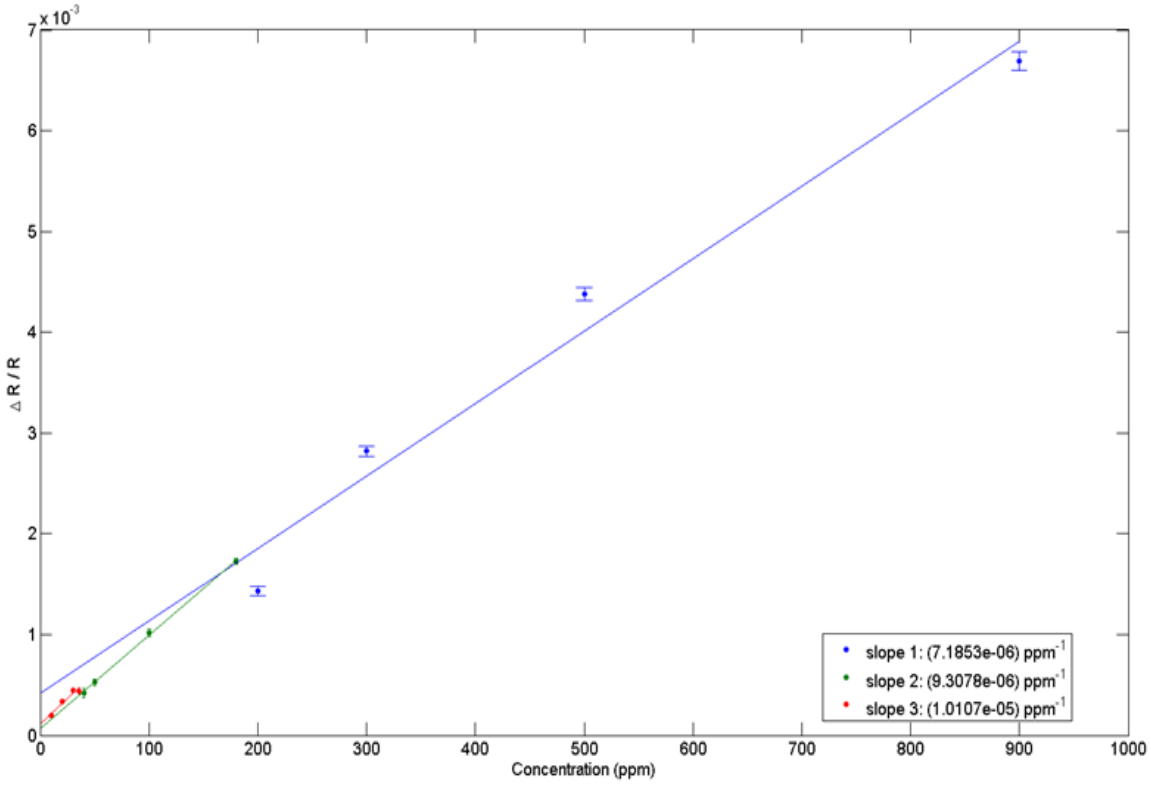

Figure 29. Sensitivity vs concentration data for Device 5 (Polystyrene-carbon black 10%) nanocomposites with varying concentrations from 10.5 ppm to 900 ppm ethanol. The lines indicated by red, green and blue colors indicate the measurements undertaken in the separate intervals of similar background flow.

3.4 Validation of reversible behavior and sensors response characteristics for ethanol at low concentrations with a known dataset

From the two independent experiments done at increasing and decreasing order of concentrations of ethanol, validation of reversibility was established. The data points from both the datasets were fitted with a straight line and the slope of the fitted lines were compared. The order of magnitude of both the slopes was found to be similar for each type of devices. Particularly, Device 4 (as shown in Figure 30), showed linear behavior characteristics for both categories of datasets. The slopes of the fitted line were found to be in close conformity. This behavior clearly indicated the reversibility exhibited by the sensors. The minor discrepancy in the slope values of the two datasets can be attributed to the uncertainty (5%) established previously in concentrations at lower values. Despite this minor discrepancy, the overall nature of the data points is linear and both lines tend to pass through/near origin if they were to be extrapolated. This behavior was also observed in Figure 29, where we saw that closer the data sets are near to the origin, the extrapolated line tends to pass exactly from the origin.

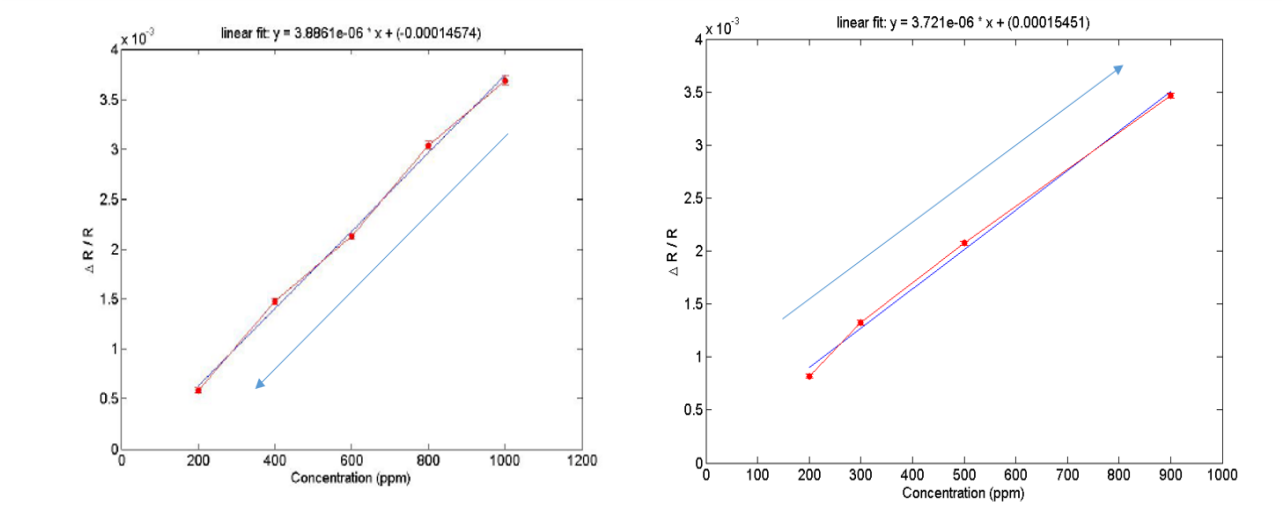

Figure 30. Sensitivities trends of devices with increasing and decreasing concentrations for Device 4 (PCL + CB 5%)

Another interesting validation can be done to see if the nature of slope remains to be linear if we observe a linear trend sub-ppm concentration regime as well, the similar behavior that we see in higher concentration region. In literature we observe that in the lower concentration ranges there is a linear trend while a less steep slope for sensitivity vs. concentrations in higher concentration ranges. Since our measurements are confined for only lower concentrations regions and that too a minute region of this lower concentration regions (as we are discussing sub-ppm concentration scale here), we refer to Lonergan et al [20] and compare our data to theirs. For the same carbon black-polymer nanocomposites (CB-PEVA), we see that the slope observed by our devices are an order of magnitude higher than theirs. This can be attributed to the fact that we use carbon black content at 10% while their devices are having 15% and 50%, thus affecting the specificity. It should further be noted that the analyte detected by them is benzene while we are measuring sensitivities of ethanol at varying concentrations. The discrepancies tend to relate well with the observations, as selectivity of CB-polymers composites differ with different analytes.

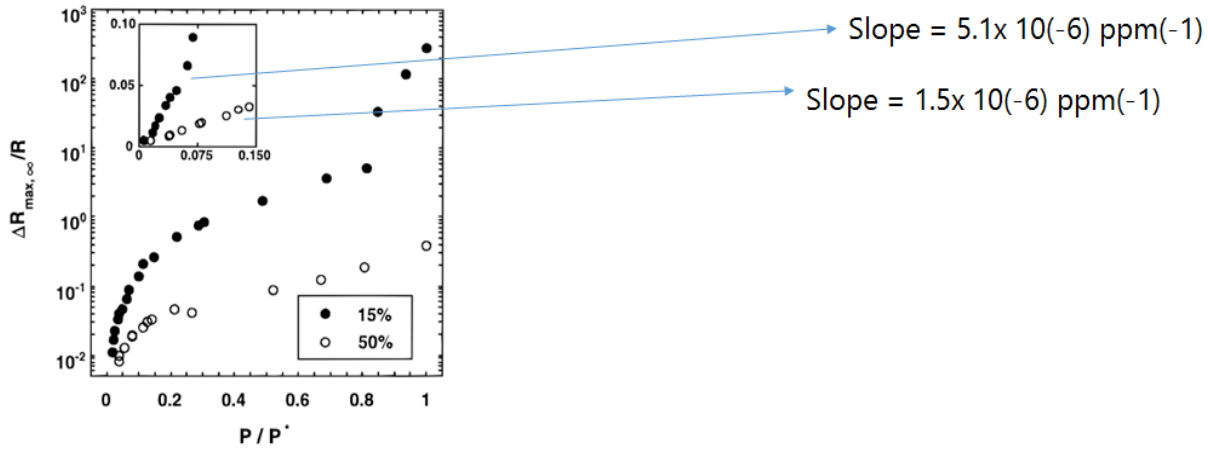

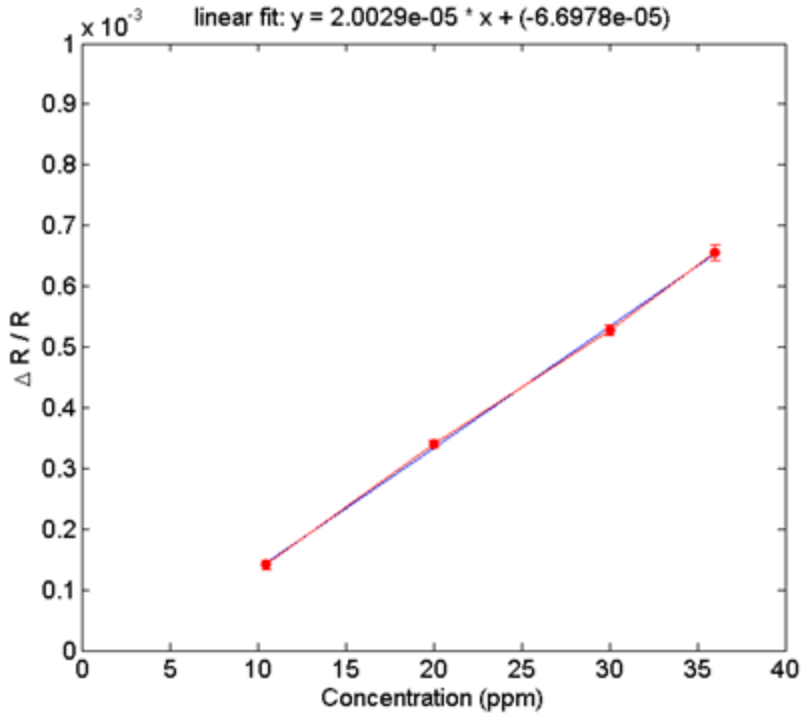

Figure 31. Comparison of slope of a typical dataset of response to VOC-Benzene (top) by Lonergan et al. (corresponding to CB-PEVA 15% for black dots and CB-PEVA 50% for white dots) [20] with that to the raw data sensor data obtained (bottom) from Device 8 (CB-PVAC 10%) sensor response towards ethanol.

3.5 Determination of limit of detection (LOD) with different analytes at low concentrations

The linear behavior exhibited by each device was utilized to evaluate LOD capability of sensor array for four analytes: ethanol, methanol, toluene and water vapor. Four sets of experiments were carried out in sub-ppm concentration ranges. The background flow kept at a same value (15000 sccm) for all the four measurements.

Since LOD is defined as the concentration where sensor response signal is three times the noise of the blank [36], we fitted a horizontal line at three times of average of vertical error bars

at each data point of that device. The linear extrapolation is valid for each device since we have seen previously and in literature ([20], [37]) that most chemiresistive sensors follow the linear behavior in low concentration ranges. Our model assumes zero signal at zero concentration, hence rather than extrapolation of the last data point nearest to the origin, we fit a line through all the points in sub-ppm concentration ranges and the origin. Limit-of-detection (LOD) values were then determined by taking the concentration value at intersection between this horizontal line and the fitted line from the last data point, assuming that all devices will tend to converge at origin linearly. Various plots at sub-ppm concentrations for different analytes are shown below. The limit of detection value for each analyte was attributed to the device that exhibited the least value among the sensor array.

The uncertainty in the values of slopes was also taken into account and this provided a range of LOD values for each analyte. The uncertainty of the slope can be estimated by how well the line fits the data points with the origin. For example, if all four points in sub-ppm concentration range and the origin fall in the same line, the uncertainty would be zero and if there is a large offset the uncertainty will be high. This was calculated by uncertainty propagation formula from [38]. The uncertainty in LOD is calculated by

$$\sigma(\text{LOD}) = \left|\frac{y_n}{m^2}\right| \sigma(m)$$

y_n = sensitivity value at limit of detection

m = slope of the fitted line

$\sigma(m)$ = uncertainty in the slope

With ethanol, except gold nanoparticles based device all devices showed sensitivity at sub-ppm concentration ranges. The inability of the gold nanoparticles based device could be attributed to aging effect and presence of high electrical noise. High noise could have occurred because of presence of too many conduction pathways between gold nanoparticles. Detection limit of graphene (as shown in Table 2) is comparable to carbon-black composite sensors. The lowest limit of detection was obtained for Device 6 (PVAC + CB 10%) at 750 ppb +/- 40 ppb.

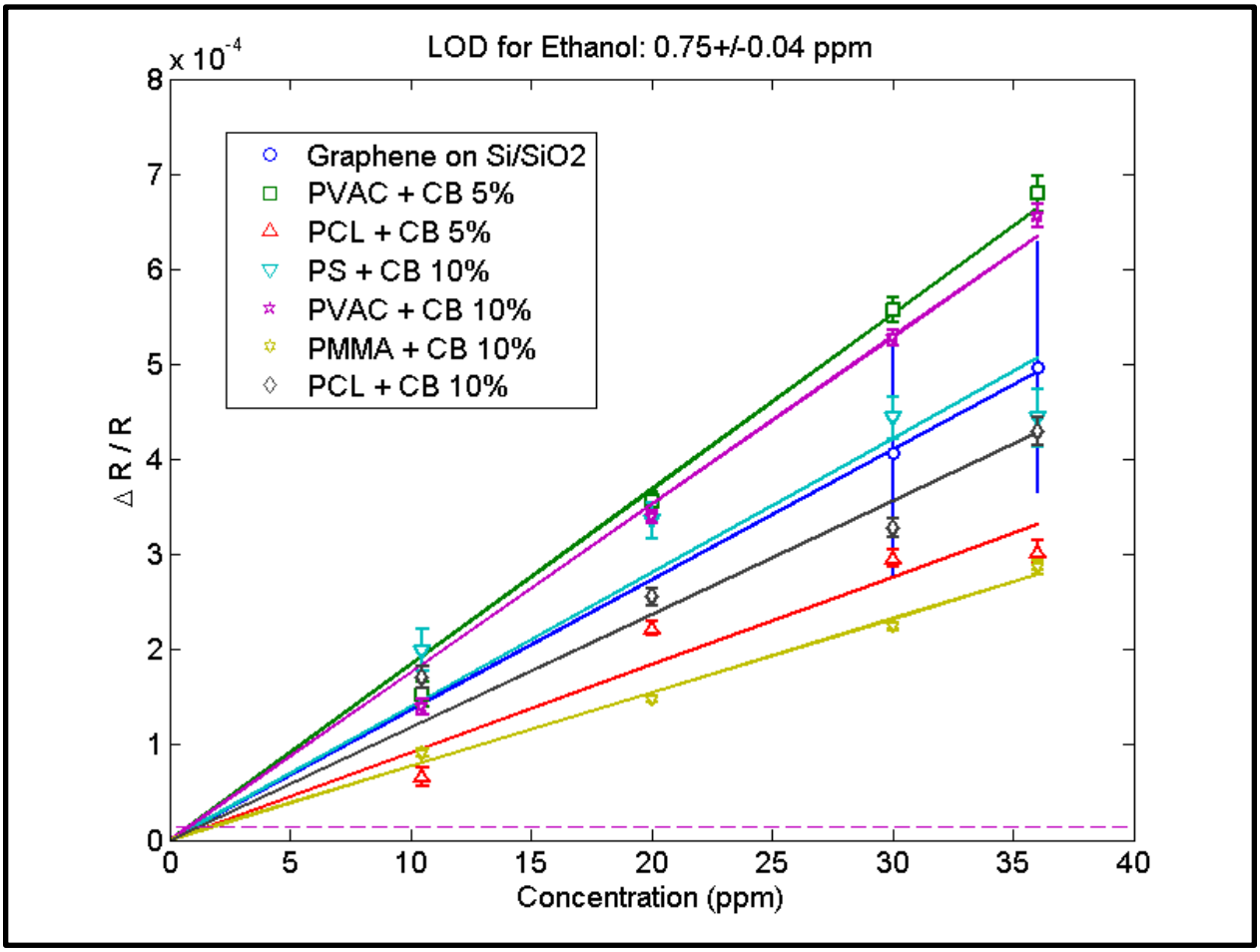

Figure 32. Sensitivity vs concentration plots for all devices that show response to ethanol in sub-ppm concentration range.

With methanol, highest selectivity and differential responses from the sensor array were obtained with only four out of total eight devices showing response at sub-ppm concentration ranges. The lowest limit of detection was shown by Device 5 (as shown in Figure 33.) having a value of 1.61 ppm +/- 0.09 ppm. Lower molecular weight of methanol as compared to ethanol could be a possible reason for good selectivity of methanol. Though, the absolute values of limit of detection are not as low as that of ethanol, the selectivity is enhanced in comparison.

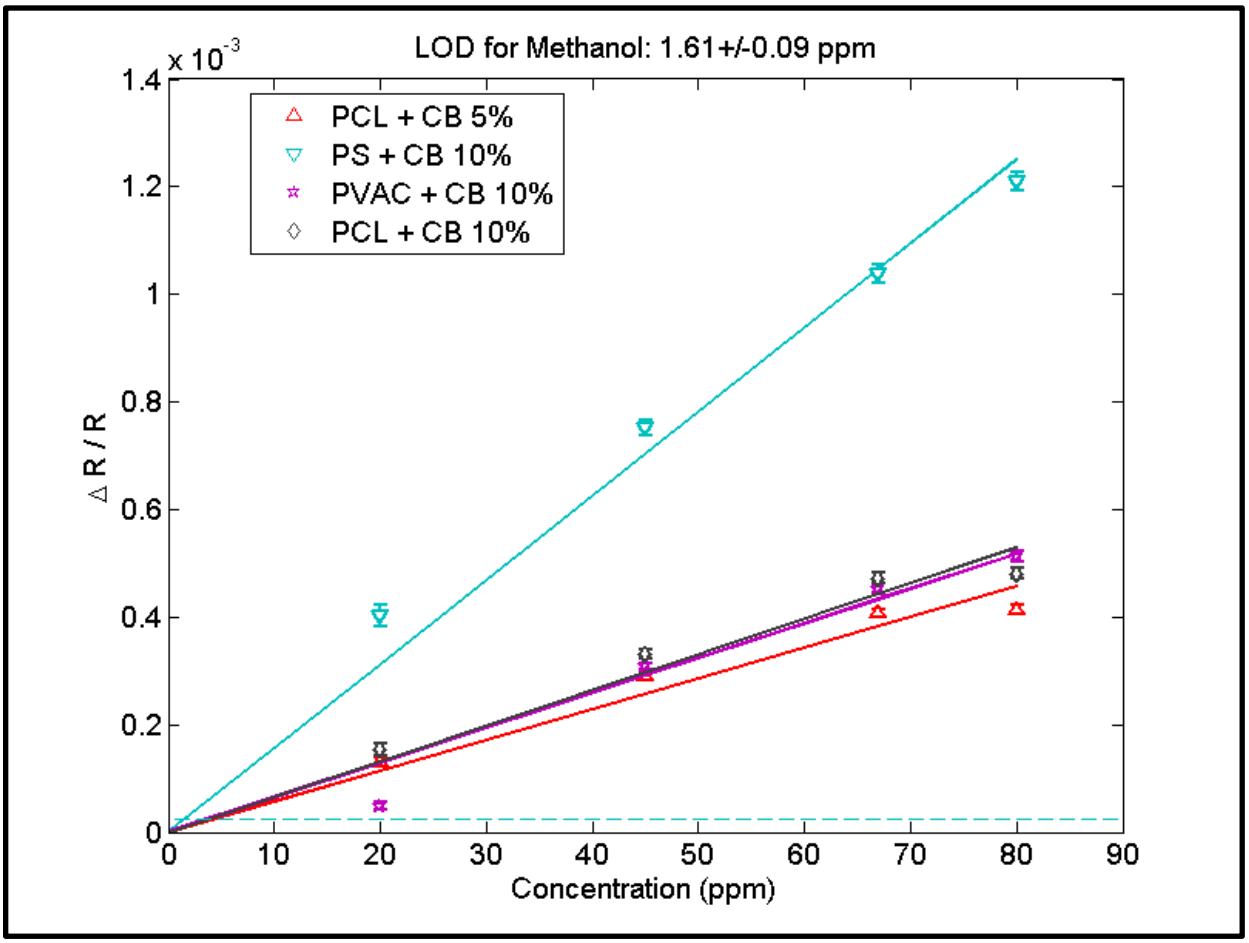

Figure 33. Sensitivity vs concentration plots for all devices that show response to methanol in sub-ppm concentration range.

With toluene, the lowest limit of detection was demonstrated by Device 4 (PCL + CB 5 %), with the value being 830 +/- 70 ppb (as shown in Figure 34.). Most devices apart from gold nanoparticles showed responses in this case. Toluene sensitivity for all the devices was found to be somewhat higher as compared to that of ethanol. For a concentration in the range of 30-35 ppm, the sensitivities of toluene were around two times higher. Though, these high sensitivities values are displayed by same devices in both the cases (PVAC + CB - 5% and 10 %).

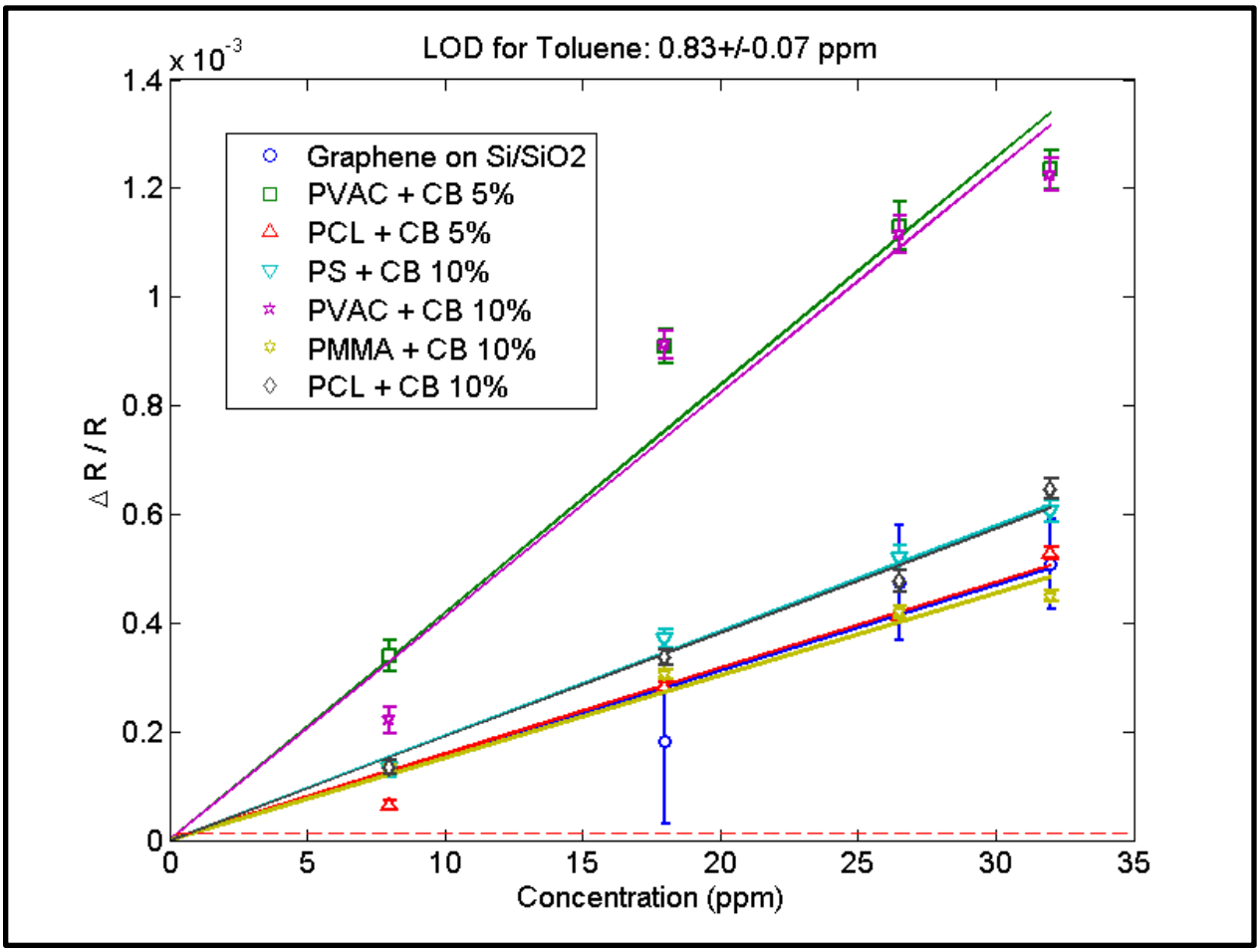

Figure 34. Sensitivity vs concentration plots for all devices that show response to methanol in sub-ppm concentration range.

With water vapor, the lowest limit of detection value was 260 ppb +/- 40 ppb with the Device 6 (CB + PVAC - 10%). The sensitivities values for water vapor was highest at this sub-ppm concentration among all other analytes. This makes the sensor array an excellent humidity sensor but at the same time limiting its applications in atmospheric conditions. Since the known signal towards humidity have been gathered, training and signal processing techniques (for eg. PCA and ANN) can help us to distinguish moisture signal vs a signal from a target analyte.

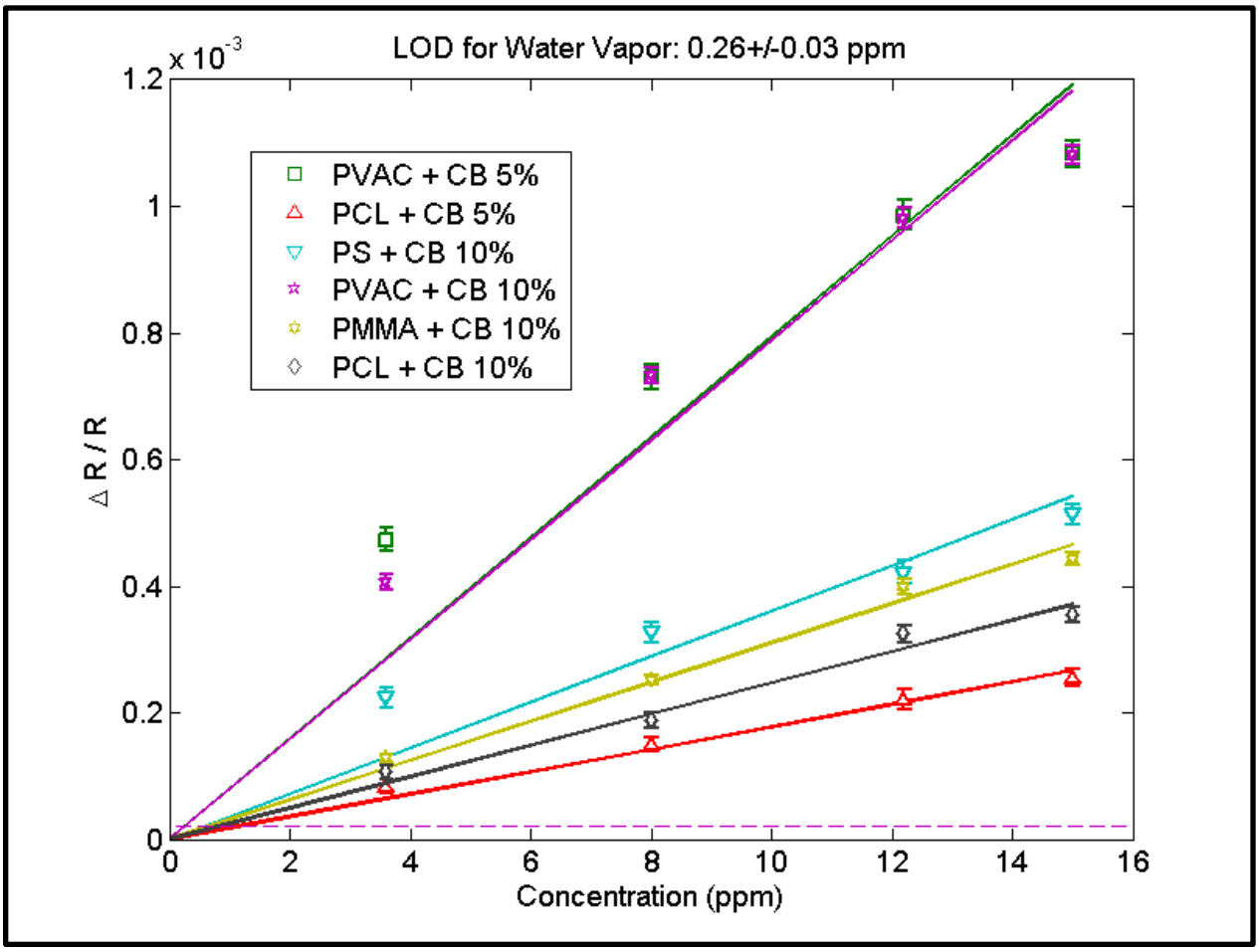

Figure 35. Sensitivity vs concentration plots for all devices that show response to methanol in sub-ppm concentration range.

The following table (Table 2) summarizes the LOD values with uncertainty for different devices (bold values indicate lowest LOD for a particular analyte) with different analytes in sub-ppm concentration ranges. The sensitivity values are indicated after the LOD values for each sensor.

Device # and composition	LOD for Ethanol (in ppm) / Sensitivity ($\times 10^{-4}$)	LOD for Methanol (in ppm) / Sensitivity ($\times 10^{-4}$)	LOD for Toluene (in ppm) / Sensitivity ($\times 10^{-4}$)	LOD for Water Vapor (in ppm) / Sensitivity ($\times 10^{-4}$)
Device 1 (Graphene on Si/SiO_2)	14.28 +/- 0.82 1.955	NR	10.86 +/- 2.67 1.70	NR
Device 2 (Au NPs with Butanethiol)	NR	NR	NR	NR
Device 3 (PVAC + CB 5 %)	1.09 +/- 0.05 0.203	NR	1.24 +/ 0.11 0.523	0.39 +/- 0.05 0.311
Device 4 (PCL + CB 5%)	1.55 +/- 0.18 0.143	1.71 +/- 0.15 0.0977	**0.83 +/- 0.07** 0.132	1.10 +/- 0.06 0.1952
Device 5 (PS + CB 10%)	2.48 +/- 0.31 0.349	**1.61 +/- 0.09** 0.2523	1.49 +/- 0.05 0.289	0.69 +/- 0.09 0.2491
Device 6 (PVAC + CB 10 %)	**0.75 +/- 0.04** 0.132	1.92 +/- 0.20 0.1244	1.04 +/- 0.11 0.431	**0.26 +/- 0.03** 0.2086
Device 7 (PMMA + CB 10 %)	0.93 +/- 0.03 0.072	NR	0.85 +/- 0.06 0.129	0.44 +/- 0.02 0.1370
Device 8 (PCL + CB 10 %)	1.41 +/- 0.12 0.167	2.12 +/- 0.17 0.1401	1.30 +/- 0.07 0.25	0.73 +/- 0.04 0.182

Table 2. Table of limit of detection (LOD) values with different analytes at low concentrations for all analytes. Since device 2 did not show any signal in low concentration, it is indicated by no response (NR).

3.6 Discussion on underlying mechanisms in behavioral patterns of all devices for different gaseous analytes at low concentrations

A comparative analysis and behavioral patterns of each individual sensor is described briefly in this section. Possible causes and underlying of characteristic/anomalies in the behavior pattern and sources of error are also discussed.

Device I, graphene on Si/SiO_2 was found to be an excellent sensor at low concentrations of ethanol. Pristine graphene has been explored in literature and it has been shown that the affinity is limited to gases or VOCs [24]. There are simulation studies being undertaken that delve into the possible transduction mechanisms of pristine graphene on different type of substrates. Some attribute sensing due to the micro-cracks on the graphene surface, the cracks acting as the sites for analytes affecting the bandgap of graphene by charge transfer mechanism [26] while others claim that it is the contaminant material during processing of graphene that acts a functionalized materials and have a say on transduction. In our case, we used PMMA to transfer graphene on the substrate. PMMA residue on graphene may be action as a functionalized agent. Adsorption of analyte molecules onto the PPMA residue could possibly be affecting the axial stresses of graphene and affecting the sensitivity. Our assumption is that a combination of both the factors can be attributed to sensitivity, though major reason being the presence of PMMA. This is regarded as the major reason because we see a similar baseline drift as other PMMA based device in parallel. The specificity towards ethanol and toluene at low

concentrations can be attributed by polymer as we know that three out of four analytes are polar in nature. The presence of large error bars in the low concentration ranges for graphene (Figure 32 and 34), indicate that data fitting gets compromised in these concentration regions. Plots of the fits indicate very high time constants for some gases, thereby effecting the quality of the fit. This indicates slower binding of the molecules on graphene device, thereby affecting time constants at low concentration.

The performance of this demonstrated is as ppm-level detection capability of pristine graphene based sensors has been limited. In our knowledge, there have been works that demonstrate graphene oxide [39], reduced graphene oxide [39] and other graphene derivatives based devices, for eg. carbon nanotubes [22] for VOCs but using pristine graphene for trace detection of VOCs has been very rare and still evolving.

In Device 2, gold nanoparticles encapsulated with butane-thiol acts as active sensing layer for detection. We don't see any response of this device in low concentration ranges. This is primarily because of high electrical noise in this region or aging. Since the charge transport mechanism in thiol capped gold nanoparticles is due to electrical hopping, it can be said that there could be too many parallel conducting paths that could be taking place which makes detection capability difficult at low concentrations of VOCs. An effective way to mitigate this problem can be baking the device prior to installation. This may disrupt many alternate conduction pathways by formations of agglomerates and defining a fixed inter particle distance.

In Devices 3 to 8, we see a linear and consistent behavior of sensitivities with concentrations for all analytes. Devices with similar polymer (but different carbon black content) have been shown to display similar affinity toward same analyte. This is primarily because the

change in resistance is directly related expanded volume by the absorbed analyte above the percolation threshold (from [21]);

$$\Delta R = kvC_{sensor}$$

where

$k =$ sensitivity factor of a composite sensor to volume change

$v =$ specific volume of analyte as a liquid

$C_{sensor} =$ concentration of analyte in sensor film

There can be many sources of error. Few of the possible sources of error are identified below:

- Inaccuracies in the mass flow controller. Since the flows were in the range of few sccms and the mass flow controllers tended to deviate from the set point, there could be uncertainty in obtained concentration values.
- Joule heating up of the sensors can lead to higher electrical noise. Joule heating may enhance random motion of particle and sudden fluctuations in the resistance. This could have been typically seen in long run experiments.
- Calibration of the digital multimeter may have led to unaccountable errors in all measurements. A systematic calibration error in the digital multimeters could have led to unaccountable error in absolute measurements of resistances. Since four wire method is being used by us, there could be calibration error in measuring either current or voltage, propagating the error in final resistance measurement.

CHAPTER 4
CONCLUSIONS

An array based gas sensing setup based on chemiresistive mechanism has been demonstrated with sensing elements ranging from carbon black-polymer nanocomposites, graphene monolayer and gold nanoparticles. Chemiresistive mechanism offers has been previously demonstrated to show very low limits of detection with VOCs. This was validated by taking sensing measurements in sub-ppm ranges for four analytes; ethanol, methanol, toluene and water vapor. Most sensors showed linear while some showed sub-linear behavior of sensitivity with concentration values. The nature of this behavior and reversibility of sensor response were validated by comparing a known dataset from literature. LOD values for each of the microsensor was evaluated by extrapolating the linear relationship of sensitivity and concentration. LOD values are comparable, if not superior to those values seen in literature. The lowest LOD was obtained for water vapor, having a value of 260 +/- 30 ppb from Device 6 (polyvinylacetate-carbon black (10%)). The next highest sensitivity was shown for ethanol, having a value of 750 +/- 40 ppb with the same device. Following this, LOD value for toluene was established to be 830 +/- 70 ppb shown by Device 4 (polycaprolactone-carbon black (5%)). Methanol, among the four analytes showed most differential response with LOD value of 1.61 +/- 0.09 ppm, shown by Device 5 (polystyrene-carbon black (10%)). The differential response can potentially be used to implement PCA and ANN techniques to demonstrate capability of an e-nose system. Adding more sensing elements by adding polymers-composites with varying composition and content, would further enhance the discrimination capability of this array. Using 4-wire measurement techniques and implementing customized fitting methods and averaging has tremendously improved the detection capability. It can be prophesized that implementing flexible substrates and vacuum system can even further enhance sensitivity values with the same sensing elements.

APPENDIX I

LabVIEW block diagram for data acquisition from digital multimeters

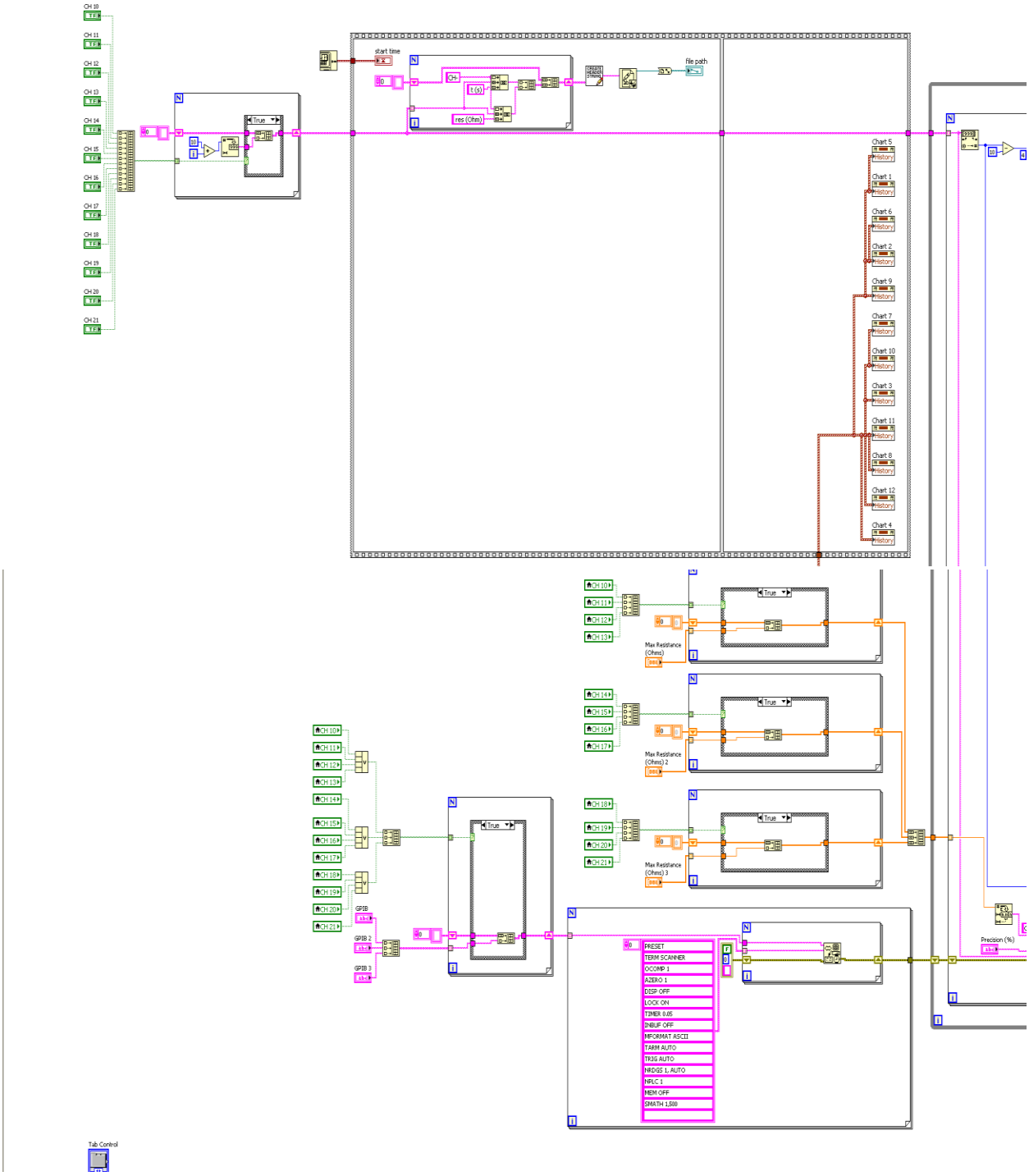

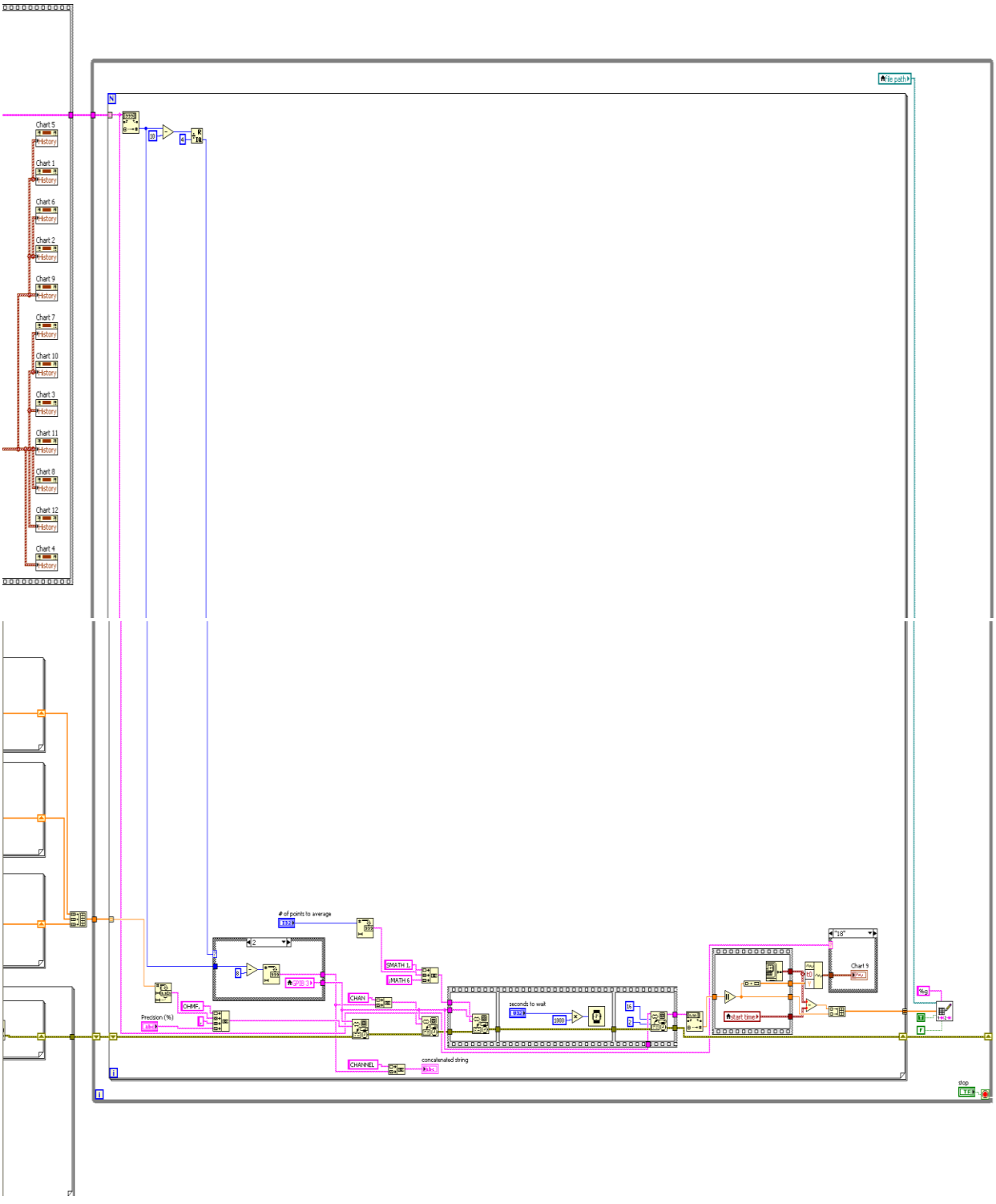
Chart 5
Chart 1
Chart 6
Chart 2
Chart 9
Chart 7
Chart 10
Chart 3
Chart 11
Chart 8
Chart 12
Chart 4
file path
# of points to average
GPIB 1
SMATH 1
MATH 6
CHAN
OHMS
Precision (%)
CHANNEL
concatenated string
seconds to wait
start time
"18"
Chart 9
stop

APPENDIX II

MATLAB code for fitting raw data to the fitting function

```
function [Rout, R_initial, background] = fit_signal_with_bg(t,t_change,concentration,R_sat,tau,BGval)
% inputs: t is the time vector.
% R_sat are the saturation resistance values. (i.e. the limit that
% the exponentials approach)
% t_change is a vector containing the start times for new
% exponentials. (i.e. when the gas concentration was changed)
% concentration is a vector containing the analyte concentrations
% Rstart & Rend are the resistance values at t(1) and t(end)
% tau is the time constant
% BGval is the size of the background signal at the t_change times.
% length(BGval) = length(t_change)+2 . (2 additional points for
% t(1) and t(end).)
if length(tau) == 1
    tau = tau*ones(1,length(concentration));
elseif length(tau) == 2
    tau1 = tau(1);
    tau2 = tau(2);
    tau = tau2*ones(1,length(concentration));
    i0 = concentration == 0;
    tau(i0) = tau1;
end

t_change = [t(1), t_change, t(end)];
xBG = t_change;
[~,~,iC] = unique(concentration);
Rout = zeros(size(t));

yBG = BGval;
if length(BGval) < length(concentration) + 1
    % background_type is 2
    zero_conc = concentration == 0;
    zero_conc(1) = 0;
    yBG = zeros(size(xBG));
    N = 1;
    for i = 1:length(zero_conc)
        if zero_conc(i) == 0
```

```
            yBG(i) = BGval(N);
            N = N + 1;
        elseif zero_conc(i) == 1
            yBG(i) = interp1([xBG(i-1),xBG(i+1)], ...
                [BGval(N-1),BGval(N)], xBG(i));
        end
    end
    yBG(end) = BGval(end);
end
background = zeros(size(t));
background(1) = BGval(1);
R0 = 0;
R_initial = zeros(size(concentration));
R_initial(1) = R0;
Rout(1) = BGval(1);
Nsegment = 1;
for i = 2:length(t)
    t0 = t_change(Nsegment);
    background(i) = yBG(Nsegment) + ...
        (yBG(Nsegment+1)-yBG(Nsegment))/(xBG(Nsegment+1)-
xBG(Nsegment))*...
        (t(i)-xBG(Nsegment));

    Rout(i) = (R0 - R_sat(iC(Nsegment)))*exp(-(t(i)-t0)/tau(Nsegment))
...
        + R_sat(iC(Nsegment)) + background(i);

    if i == length(t)
        break
    else
    if t(i+1) > t_change(Nsegment+1)
        R0 = Rout(i) - background(i);
        Nsegment = Nsegment + 1;
        R_initial(Nsegment) = Rout(i);
    end
    end
end

R_initial = R_initial(1:end-1)
```

APPENDIX III

MATLAB code for importing the text file and extracting data, performing the fit, calculating sensitivity, plotting and storing plots of sensitivity and concentration values.

```
% ***** only edit these three lines below *****
device_number = 1; % Choose the device number (1 -> 8).
remove_start_time = 0; % Use this to delete unwanted data points.
remove_stop_time  = 0; % Start time and stop time are in minutes.
% ******************************************

file = uigetfile('.txt');
data = importdata(file);
data = data.data;

column_number = device_number * 2 - 1;
x = data(:,column_number)/60; % convert x values to minutes
y = data(:,column_number + 1);

points_to_remove = x > remove_start_time & x < remove_stop_time;
x(points_to_remove)=[];
y(points_to_remove)=[];

x(1:50) = [];
y(1:50) = [];

y = 100*(y/y(1)); % convert y values to percentage

x(end) = [];
y(end) = [];

figure;
plot(x,y,'k','linewidth',2)
set(gca,'fontsize',16,'linewidth',1);
xlabel('time (minutes)');
ylabel('% Resistance');
set(gcf,'color','white')

titles = ...
    {'Dev 1 (Graphene on Si/SiO2)';
     'Dev 2 (Gold NPs capped with butanethiol)';
```

```
     'Dev 3 (Carbon Black - Polyvinyl Acetate-5%)';
     'Dev 4 (Carbon Black - Polycaprolactone-5%)';
     'Dev 5 (Carbon Black - Polystyrene-5%)';
     'Dev 6 (Carbon Black - Polyvinyl Acetate-10%)';
     'Dev 7 (Carbon Black - PMMA-10%)';
     'Dev 8 (Carbon Black - Polycaprolactone-10%)'};

%%
% Enter the times that you changed the gas concentration here:

%t0 = [20.8, 28.5, 38.8, 51, 60.4, 70.3, 78.4, 85.1];
%t0 = [70.16, 82.28, 93.39, 102, 114.6, 124.2];
%t0 = [29.32, 39.92, 49.51, 58.1, 68.21, 77.8, 89.42, 98.51, 110.6,
118.2, 128.8, 137.4];
%t0 = [25.26, 33.81, 59.42, 67.06, 85.04, 95.38, 107.1, 116.5, 129.5,
136];
t0 = [41.06, 56.45, 77.27, 99, 111.5, 127.7, 138.1, 151.1, 168.8,
190.5, 208.1];
% Enter the concentrations you used here (including 0 concentration
% values):
%concentration = [ 0, 20, 0, 15, 0, 10, 0];
%concentration = [0, 10.5, 0, 20, 0, 30, 0, 36, 0];%, 0, 20, 0, 15,
0];
%concentration = [0, 200, 0, 160, 0, 120, 0, 80, 0, 40, 0];
concentration = [ 0, 1000, 0, 800, 0, 600, 0, 400, 0, 200, 0];

tau = [10, 10];        % approximate time constants for exponential
rises and falls
delta_t = 2;         % wiggle-room in t0 values
background_type = 2; % this must be either 1 or 2

%-------------------------------------------------------------------
-----

BG = zeros(size(t0));
for i = 1:length(t0)
    [~,n] = min(abs(x-t0(i)));
    BG(i) = y(n);
end
BG = [y(1), BG, y(end)];
```

```
[Conc,iA,iC] = unique(concentration);
if background_type == 2
    zero_conc = concentration == 0;
    zero_conc(1) = 0;
    BG(zero_conc) = [];
end
N1 = length(iA);
N2 = length(BG);
N3 = length(t0);

fitfun = @(p,x) fit_signal_with_bg(x, p(N1+N2+3:N1+N2+N3+2), ...
    concentration, p(1:N1), p(N1+1:N1+2), p(N1+3:N1+N2+2));

p0 = [zeros(1,N1), tau, BG, t0];
lb = [zeros(1,N1), zeros(size(tau)), zeros(1,N2), t0 - delta_t];
ub = [200*ones(1,N1), 10*tau, 200*ones(1,N2), t0 + delta_t];

pout = lsqcurvefit(fitfun,p0,x,y,lb,ub);
[yfit,~,bgfit] = fitfun(pout,x);

p02 = pout(1:N1+2);
BGval = pout(N1+3:N1+N2+2);
tvals = pout(N1+N2+3:N1+N2+N3+2);
fitfun2 =@(p,x) fit_signal_with_bg(x, tvals, concentration, p(1:N1),
...
    p(N1+1:N1+2), BGval);

[pout2, resid, jacob, covarb] = nlinfit(x,y,fitfun2,p02);
conf_pout2 = nlparci(pout2,resid,'covar',covarb);
[ypred, delta] = nlpredci(fitfun2,x,pout2,resid,'covar',covarb);

upper = ypred+delta;
lower = ypred-delta;

t0 = [t0, x(end)];
Rsat = pout2(1:N1);
tau = pout2(N1+1:N1+2);
%BGval = pout2(N1+3:N1+N2+2);
%tvals = pout2(N1+N2+3:N1+N2+N3+2);
```

```
Rsat2 = pout2(1:N1);
RsatL = conf_pout2(1:N1,1);
RsatU = conf_pout2(1:N1,2);

fsz = 14;
lw = 2;
msz = 15;
figure; hold on;
hd = plot(x,y,'k','linewidth',lw);
hf2 = plot(x,bgfit,'b','linewidth',lw);
hf1 = plot(x,yfit,'r','linewidth',lw);
%hf1 = plot(x,ypred,'r','linewidth',lw);
%plot(x,upper,'--k','linewidth',lw);
%plot(x,lower,'--k','linewidth',lw);

hf3 = plot(x,yfit-bgfit+BGval(1),'--r','linewidth',lw-0.5);
hsat= plot([tvals, x(end)],Rsat(iC)+BGval(1),'.k','markersize',msz);
set(gca,'fontsize',fsz,'linewidth',1);
xlabel('Time (minutes)')
ylabel('% Resistance')
box on;
set(gcf,'color','w')

legend([hd,hf1,hf2,hf3,hsat],{'data','fit','background','fit          -
background'...
    'saturation values'},'location','north');

title([titles{device_number},',  rise  time  const:  ',num2str(tau(2)),'
minutes',...
    ', decay time const: ',num2str(tau(1)),' minutes']);

Conc = Conc(2:end);
delta_R = (Rsat(2:end) - Rsat(1)) / 100;
delta_R2= (Rsat2(2:end) - Rsat2(1))/100;
errL= delta_R2' - (RsatL(2:end) - Rsat2(1))/100;
errU=-delta_R2' + (RsatU(2:end) - Rsat2(1))/100;
figure; hold on;
plot(Conc,delta_R,'.-','markersize',20,'linewidth',1);
errorbar(Conc,delta_R2,errL,errU,'.-r','markersize',20,'linewidth',1);
```

```
box on;
set(gca,'fontsize',14);
xlabel('Concentration (ppm)');
ylabel('\Delta R / R');
set(gcf,'color','white');
ax = axis;
axis([0 ax(2) 0 ax(4)]);
%dx = ax(2)-ax(1);
%dy = ax(4)-ax(3);
%axis([ax(1)-dx*0.05, ax(2)+dx*0.05, ax(3)-dy*0.05, ax(4)+dy*0.05]);

disp(['time constant for pure N2: ',num2str(tau(1)),' minutes']);
disp(['time constant for analyte: ',num2str(tau(2)),' minutes']);

clearvars -except 'concentration_all' 'delta_R_all' 'Conc' 'delta_R'
...
    'x' 'y' 'device_number' 'column_number' 'data' 'file' ...
    'points_to_remove'     'remove_start_time'     'remove_stop_time'
'titles' ...
    'conf_pout' 'pout2' 'pout' 'errL' 'errU' 'errL_all' 'errU_all'

%% Run this portion to create the larger arrays of data

if exist('concentration_all','var');
    L1 = length(Conc);
    L2 = size(concentration_all,1);
    N = size(concentration_all,2);
    if L2 < L1
        NaNmat = NaN*ones(L1-L2,N);
        concentration_all = [[concentration_all; NaNmat], Conc'];
        delta_R_all = [[delta_R_all; NaNmat], delta_R'];
        errL_all = [[errL_all; NaNmat], errL];
        errU_all = [[errU_all; NaNmat], errU];
    elseif L2 > L1
        NaNmat = NaN*ones(L2-L1,1);
        concentration_all = [concentration_all, [Conc'; NaNmat]];
        delta_R_all = [delta_R_all, [delta_R'; NaNmat]];
        errL_all = [errL_all, [errL; NaNmat]];
        errU_all = [errU_all, [errU; NaNmat]];
    elseif L2 == L1
```

```
        concentration_all = [concentration_all, Conc'];
        delta_R_all   = [delta_R_all, delta_R'];
        errL_all = [errL_all, errL];
        errU_all = [errU_all, errU];
    end
else
    concentration_all = Conc';
    delta_R_all   = delta_R';
    errL_all = errL;
    errU_all = errU;
end

%% Run this portion to plot delta_R over R for all the data

xdata = reshape(concentration_all, numel(concentration_all), 1);
ydata = reshape(delta_R_all, numel(delta_R_all), 1);
xdata = xdata(isnan(xdata)==0);
ydata = ydata(isnan(ydata)==0);
fitfun =@(p,x) p*x;
pout = nlinfit(xdata,ydata,fitfun,0);
%p_fit = polyfit(xdata,ydata,1);
xfit = [0; sort(xdata)];
%yfit = polyval(p_fit,xfit);
yfit = fitfun(pout,xfit);

figure; hold on;
%plot(concentration_all, delta_R_all, '.', ...
%    'markersize',20,'linewidth',1);
errorbar(concentration_all,delta_R_all,errL_all,errU_all,'.', ...
    'markersize',15,'linewidth',1);

plot(xfit, yfit,'linewidth',1);
set(gca,'fontsize',14);
xlabel('Concentration (ppm)');
ylabel('\Delta R / R');
set(gcf,'color','white');
box on;
ax = axis;
axis([0 ax(2) 0 ax(4)]);
```

```
title(['linear fit: y = ',num2str(p_fit(1)),' * x + ',num2str(p_fit(2))]);

%%
filename = 'DATA_device_8.mat';
save(filename, 'concentration_all', 'delta_R_all', 'xfit', 'yfit','errL_all','errU_all');
```

References

1. Peng, Gang et al. "Diagnosing Lung Cancer in Exhaled Breath Using Gold Nanoparticles". *Nature Nanotech* 4.10 (2009): 669-673.
2. Gavgani, Jaber Nasrollah et al. "A Room Temperature Volatile Organic Compound Sensor With Enhanced Performance, Fast Response And Recovery Based On N-Doped Graphene Quantum Dots And Poly(3,4-Ethylenedioxythiophene)–Poly(Styrenesulfonate) Nanocomposite" RSC Adv. 5.71 (2015): 57559-57567.
3. Weerakoon, Kanchana A and Bryan A Chin. "A Chemical Switch For Detecting Insect Infestation". Pest. Manag. Sci. 68.6 (2012).
4. Baller, M.K et al. "A Cantilever Array-Based Artificial Nose". *Ultramicroscopy* 82.1-4 (2000): 1-9.
5. Yamagiwa, H., Sato, S., Fukawa, T., Ikehara, T., Maeda, R., Mihara, T. and Kimura, M. (2014). Detection of Volatile Organic Compounds by Weight-Detectable Sensors coated with Metal-Organic Frameworks. Sci. Rep., 4, p.6247.
6. Ellern, I., Hesketh, P., Stavila, V., Lee, J., Allendorf, M., Venkatasubramanian, A. and Robinson, A. (2013). HKUST-1 coated piezoresistive microcantilever array for volatile organic compound sensing. Micro & Nano Letters, 8(11), pp.766-769.
7. Clevenson, Hannah et al. "High Sensitivity Gas Sensor Based On High-Q Suspended Polymer Photonic Crystal Nanocavity". *Appl. Phys. Lett.* 104.24 (2014): 241108.

8. Joe, Daniel J. et al. "Stress-Based Resonant Volatile Gas Microsensor Operated Near the Critically Buckled State". *J. Appl. Phys.* 111.10 (2012): 104517.
9. Groves, W. A., A. B. Grey, and P. T. O'Shaughnessy. "Surface Acoustic Wave (SAW) Microsensor Array for Measuring Vocs In Drinking Water". J. Environ. Monit. 8.9 (2006): 932-941.
10. Bur, Christian et al. "Detecting Volatile Organic Compounds in The Ppb Range with Gas Sensitive Platinum Gate Sic-Field Effect Transistors". IEEE Sensors J. 14.9 (2014): 3221-3228.
11. Paska, Yair et al. "Enhanced Sensing of Nonpolar Volatile Organic Compounds by Silicon Nanowire Field Effect Transistors". ACS Nano 5.7 (2011): 5620-5626.
12. Chen, B., Liu, H., Li, X., Lu, C., Ding, Y. and Lu, B. (2012). Fabrication of a graphene field effect transistor array on microchannels for ethanol sensing. Applied Surface Science, 258(6), pp.1971-1975.
13. Torsi, Luisa et al. "Organic Field-Effect Transistor Sensors: A Tutorial Review". Chemical Society Reviews 42.22 (2013): 8612.
14. Chiu, Shih-Wen and Kea-Tiong Tang. "Towards A Chemiresistive Sensor-Integrated Electronic Nose: A Review". Sensors 13.10 (2013): 14214-14247.
15. Kahn, Nicole et al. "Dynamic Nanoparticle-Based Flexible Sensors: Diagnosis of Ovarian Carcinoma from Exhaled Breath". Nano Letters 15.10 (2015): 7023-7028.

16. Li, Zhipeng et al. "Porous Sno2 Nanospheres as Sensitive Gas Sensors for Volatile Organic Compounds Detection". Nanoscale 3.4 (2011): 1646.
17. Inyawilert, K. et al. "Rapid Ethanol Sensor Based On Electrolytically-Exfoliated Graphene-Loaded Flame-Made In-Doped Sno2 Composite Film". Sensors and Actuators B: Chemical 209 (2015): 40-55.
18. Skotadis, E. et al. "Platinum Nanoparticle Chemical Sensors On Polyimide Substrates". *Procedia Engineering* 47 (2012): 778-781. Web.
19. Franke, Marion E., Tobias J. Koplin, and Ulrich Simon. "Metal and Metal Oxide Nanoparticles In Chemiresistors: Does The Nanoscale Matter?". Small 2.3 (2006): 301-301.
20. Lonergan, Mark C. et al. "Array-Based Vapor Sensing Using Chemically Sensitive, Carbon Black−Polymer Resistors". Chemistry of Materials 8.9 (1996): 2298-2312.
21. Kang, Nae Kyoung et al. "Evaluation of The Limit-Of-Detection Capability of Carbon Black-Polymer Composite Sensors for Volatile Breath Biomarkers". Sensors and Actuators B: Chemical 147.1 (2010): 55-60.
22. Chatterjee, S., M. Castro, and J. F. Feller. "An E-Nose Made of Carbon Nanotube Based Quantum Resistive Sensors for The Detection of Eighteen Polar/Nonpolar VOC Biomarkers of Lung Cancer". Journal of Materials Chemistry B 1.36 (2013): 4563.
23. Bai, Hua and Gaoquan Shi. "Gas Sensors Based On Conducting Polymers". Sensors 7.3 (2007): 267-307.

24. Varghese, S., Lonkar, S., Singh, K., Swaminathan, S. and Abdala, A. (2015). Recent advances in graphene based gas sensors. Sensors and Actuators B: Chemical, 218, pp.160-183.
25. Kumar, S., Kaushik, S., Pratap, R. and Raghavan, S. (2015). Graphene on Paper: A Simple, Low-Cost Chemical Sensing Platform. ACS Appl. Mater. Interfaces, 7(4), pp.2189-2194.
26. Smith, A., Elgammal, K., Niklaus, F., Delin, A., Fischer, A., Vaziri, S., Forsberg, F., Råsander, M., Hugosson, H., Bergqvist, L., Schröder, S., Kataria, S., Östling, M. and Lemme, M. (2015). Resistive graphene humidity sensors with rapid and direct electrical readout. Nanoscale, 7(45), pp.19099-19109.
27. Walker Jr., P. and Kotlensky, W. (1962). APPARENT DENSITIES AND INTERNAL SURFACE AREAS OF SELECTED CARBON BLACKS. Canadian Journal of Chemistry, 40(2), pp.184-188
28. Zhang, Y., Zhang, L. and Zhou, C. (2013). Review of Chemical Vapor Deposition of Graphene and Related Applications. Accounts of Chemical Research, 46(10), pp.2329-2339.
29. A. K. and C. H. Lee, "Synthesis and biomedical applications of graphene: present and future trends," Advances in Graphene Science, Jul. 2013. [Online]. Available: http://www.intechopen.com/books/advances-in-graphene-science/synthesis-andbiomedical-applications-of-graphene-present-and-future-trends.
30. Brust, M., Walker, M., Bethell, D., Schiffrin, D. and Whyman, R. (1994). Synthesis of thiol-derivatised gold nanoparticles in a two-phase Liquid–Liquid system. J. Chem. Soc., Chem. Commun., 0(7), pp.801-802.

31. Deepak, F., Mayoral, A. and Arenal, R. (n.d.). Advanced transmission electron microscopy.
32. Jena, D., Banerjee, K. and Xing, G. (2014). 2D crystal semiconductors: Intimate contacts. Nature Materials, 13(12), pp.1076-1078.
33. Kim, Y., Ha, S., Yang, H. and Kim, Y. (2007). Gas sensor measurement system capable of sampling volatile organic compounds (VOCs) in wide concentration range. Sensors and Actuators B: Chemical, 122(1), pp.211-218.
34. Ddbonline.ddbst.com. (2016). Vapor Pressure Calculation by Antoine Equation. [online] Available at: http://ddbonline.ddbst.com/AntoineCalculation/AntoineCalculationCGI.exe [Accessed Jul. 2016]
35. Arshak, K., Moore, E., Lyons, G., Harris, J. and Clifford, S. (2004). A review of gas sensors employed in electronic nose applications. Sensor Review, 24(2), pp.181-198.
36. MacDougall, D., Crummett, W. and et al., (1980). Guidelines for data acquisition and data quality evaluation in environmental chemistry. Analytical Chemistry, 52(14), pp.2242-2249.
37. Lewis, N. (2004). Comparisons between Mammalian and Artificial Olfaction Based on Arrays of Carbon Black−Polymer Composite Vapor Detectors. Accounts of Chemical Research, 37(9), pp.663-672.
38. Rit.edu. (2016). Uncertainties and Error Propagation. [online] Available at: http://www.rit.edu/cos/uphysics/uncertainties/Uncertainties.html [Accessed Jul. 2016].
39. Some, S., Xu, Y., Kim, Y., Yoon, Y., Qin, H., Kulkarni, A., Kim, T. and Lee, H. (2013). Highly Sensitive and Selective Gas Sensor Using Hydrophilic and Hydrophobic Graphenes. Sci. Rep., 3.